Effectiveness Enhancement and Reactant Depletion in a Partially Wetted Catalyst

A one-dimensional model is developed to describe reaction between a nonvolatile liquid reactant and a dissolved gas reactant in an isothermal catalytic pellet partially wetted by a flowing liquid film. The kinetics are assumed to be first order and zero order with respect to the dissolved gas and liquid reactant, respectively. The model applies to cases in which there are negligible intraparticle gradients in the direction normal to the wetted surface. A modification of the overall transport coefficients enables the model to approximate cases in which these gradients are important, for both washcoated and uniformly impregnated catalysts. The analytical solutions enable an efficient examination of the interplay between the reaction and several mass transport processes. Conditions are determined for which the catalyst effectiveness is maximized at an intermediate wetting efficiency. It is shown that the maximum is a result of two counteracting processes. As the wetting efficiency is decreased from unity the effectiveness increases if the supply of the gas reactant is more effective on the nonwetted than the wetted part; i.e., effectiveness enhancement. However, if the wetting efficiency is sufficiently reduced, the excess liquid reactant depletes within the pellet, resulting in a decreased effectiveness. A criterion is derived that predicts the minimal activity necessary to initiate depletion of the liquid reactant for a given wetting efficiency. This is useful for determining the conditions for which the common literature assumption of an excess liquid reactant is violated. The model shows good agreement with published data in which the overall rate exhibits a maximum for an intermediate liquid flow rate.

M. P. Harold, Ka M. Ng
Department of Chemical Engineering
University of Massachusetts
Amherst, MA 01003

Introduction

The problem of diffusion and reaction in a partially wetted catalytic pellet is encountered in a cocurrent gas-liquid downflow trickle-bed reactor operating in the trickling flow regime. In this regime only a fraction of the external catalyst surface may be covered by liquid, which is in the form of films, rivulets, pendular structures, and liquid pockets (Sato et al., 1973; Ng, 1986; Zimmerman and Ng, 1986). The remaining interstitial void space is occupied by the gas phase. The internal catalyst void volume is generally found to be filled with the liquid phase because of strong capillary forces (Schwartz et al., 1976).

Correspondence concerning this paper should be addressed to M. P. Harold.

A number of experimental studies of the dependence of the overall rate on the extent of wetting have appeared (Sedricks and Kenney, 1973; Germain et al., 1978; Herskowitz et al., 1979; Mata and Smith, 1981). An interesting common feature among the data is that under some conditions the global rate was found to increase as the liquid flow rate, and consequently the wetting efficiency, decreased. A plausible explanation for this observation has been offered previously (Herskowitz et al., 1979) and is here briefly summarized.

Consider a catalytic gas-liquid reaction in which the dissolved gas species is the limiting reactant and the overall rate is external mass-transfer controlled. The gas reactant mass transfer rate is higher on the nonwetted part of the pellet because the liquid that wets part of the surface constitutes an additional

resistance. As a result, the overall rate increases with decreasing wetting efficiency due to a net increase in the supply rate of dissolved gaseous reactant. The primary objective of this work is to develop a model that predicts this enhancement of effectiveness by partial wetting. In this study we do so for a washcoated catalyst on an impermeable core or a uniformly impregnated catalyst.

Several theoretical studies of reaction in a partially wetted pellet have appeared (Ramachandran and Smith, 1979; Mills and Dudukovic, 1979; Herskowitz et al., 1979; Tan and Smith, 1980; Herskowitz, 1981; Goto et al., 1981; Sakornwimon and Sylvester, 1982; Ring and Missen, 1986; among others). Despite the differences in the models and solution methods, all these studies assumed that either the liquid or the dissolved gas reactant is in excess throughout the entire pellet. Consequently, a rate expression was assumed to be zero order with respect to the excess reactant.

In the case of a gas-reactant limited reaction the assumption of zero-order dependence on the liquid reactant is reasonable if the liquid phase contains a large excess of the liquid reactant, and if the overall rate is reaction-controlled. However, the assumption's validity is questionable if the liquid reactant concentration is not in large excess of the stoichiometric requirements, which is the case for many hydrodesulfurization reactions (Gates et al., 1979), or for extremely fast, external mass-transfer limited reactions for which liquid reactant depletion may occur, such as noble metal catalyzed olefin hydrogenations.

To be more specific, consider a pellet on which the wetting efficiency is very low. The assumed nonvolatile liquid reactant must diffuse from this supply point throughout the entire pellet. Under these conditions the liquid reactant may not be in ample supply in the intrapellet region well away from the wetted surface. In fact, as our model demonstrates, the liquid reactant may deplete for a sufficiently fast reaction that is zero order in this reactant. This depletion effect has not been accounted for in any previous model except for the work of Beaudry et al. (1985). Thus, a secondary objective of this work is to determine the conditions that result in a depletion of the liquid reactant in a partially wetted pellet, and to check the impact that this depletion has on the effectiveness.

Model Formulation and Solution

Depicted in Figure 1 is a catalytic pellet of half-width $S/2$, thickness δ, and length L. This geometry models catalysts in which the reaction occurs in a thin surface shell of thickness δ. The pellet pore volume is assumed to be liquid filled because of strong capillary forces. A fraction of the outer pellet surface is wetted by a liquid film containing the nonvolatile liquid reactant B, the dissolved reactant A, reaction products, and possibly a solvent, with the wetting efficiency denoted by E_w. The pellet is surrounded by an atmosphere containing the gaseous reactant with a uniform bulk partial pressure p_{bA}. Both gas-side and liquid-side external mass transfer resistances are assumed to exist.

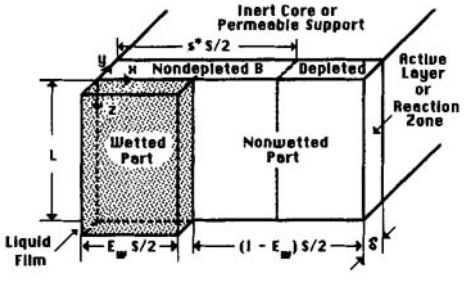

Figure 1. Slab type catalytic pellet partially wetted by a flowing liquid film.

Only half of pellet is shown. Pellet is either a washcoated catalyst with corresponding active layer of thickness δ on an inert, impermeable core, or a uniformly active catalyst with a reaction zone of thickness $\delta = V_p/S_x$.

The isothermal catalytic reaction

$$A_{(g)} + \nu B_{(\ell)} \rightarrow \text{Products}_{(\ell)}$$

where g and ℓ denote gas and liquid, respectively, has a rate (r) that is first (zero) order with respect to A (B); i.e.,

$$r = kC_A H(C_B) \tag{1}$$

where H is the Heaviside function. The advantages and limitations of the zero-order dependence on the liquid reactant are considered in the Discussion section.

Because of the thin shell geometry, as an approximation we assume that species A and B intraparticle concentrations are uniform in the direction y normal to the wetted surface. This limits the exact applicability of the model to a thinly washcoated catalyst on an impermeable core but also, as we show below, to a uniformly impregnated catalyst in which the reaction occurs in a surface shell of thickness δ. For uniformly impregnated catalysts δ is the characteristic diffusion length, V_p/S_x, where V_p is the pellet volume and S_x the external surface area. In all the cases the width S is the length of the pellet perimeter. S must be sufficiently larger than δ to justify the ignorance of curvature effects. Formally, the uniformity assumption is valid only if

$$\phi_y \triangleq \delta\sqrt{\frac{k}{D_{Ae}}} < 0.1 \tag{2}$$

is satisfied, where D_{Ae} is the effective diffusivity for A, and ϕ_y is the Thiele modulus based on the active shell thickness δ. In the event that the criterion of Eq. 2 is violated, then intraparticle gradients in the y direction exist. In this case we will retain the uniformity assumption, realizing that the concentration represents some average value of the true profile in the y direction at a fixed x location. Our approach is outlined below.

We have two key reasons for assuming a constant concentration in the y direction. First, we maintain that diffusion within the washcoat in the direction x parallel to the wetted surface is the critical one for communication between the wetted and nonwetted regions. This is especially true as the aspect ratio, $\alpha = S/2\delta$, becomes large. Second, the model solution is significantly simplified—an analytical solution is obtainable—enabling an efficient inspection of the interplay between the various rate processes. We consider the two-dimensional, bimolecular kinetics model in a future study (Funk et al., 1987). Note that our formulation is rather different from the presented work of Beaudry et al. (1985). They considered a pellet totally wetted on one side and nonwetted on the other, with liquid reactant depletion occurring at an intermediate location between the two surfaces; this corresponds to the y direction in our model.

With the assumptions in mind, the governing steady state material balances and boundary conditions are now described. Region 1 ($0 < s < E_w$) corresponds to the wetted part of the pellet. Species A and B respectively satisfy

$$\frac{d^2u_{A1}}{ds^2} + \alpha Bi_{A1}(1 - u_{A1}) - \phi^2 u_{A1} = 0 \tag{3}$$

$$\frac{d^2u_{B1}}{ds^2} + \alpha Bi_B(u_{Bf} - u_{B1}) - m\phi^2 u_{A1} = 0 \tag{4}$$

Region 2 ($E_w < s < s^*$) corresponds to the nonwetted part of the pellet (s^* is defined below). Species A and B respectively satisfy

$$\frac{d^2u_{A2}}{ds^2} + \alpha Bi_{A2}(1 - u_{A2}) - \phi^2 u_{A2} = 0 \tag{5}$$

$$\frac{d^2u_{B2}}{ds^2} - m\phi^2 u_{A2} = 0. \tag{6}$$

The dimensionless variables are defined as

$$u_{Aj} = \frac{C_{Aj}}{C_{Ae}}\,(j = 1, 2) \quad u_{Bj} = \frac{C_{Bj}}{C_{Ae}}\,(j = 1, 2)$$
$$s = \frac{2x}{S} \quad Bi_{Aj} = \frac{k_{Aj}S}{2D_{Ae}}\,(j = 1, 2) \quad Bi_B = \frac{k_BS}{2D_{Be}}$$
$$\phi^2 = \left(\frac{S}{2}\right)^2 \frac{k}{D_{Ae}} \quad \alpha = \frac{S}{2\delta} \quad m = \frac{\nu D_{Ae}}{D_{Be}} \quad u_{Bf} = \frac{C_{Bf}}{C_{Ae}} \tag{7}$$

Equations 3 and 4 account for species A and B external transport into region 1 with subsequent intraparticle diffusion in the s direction and reaction. Equation 5 accounts for species A external transport and intraparticle diffusion and reaction in region 2. Equation 6 accounts for the nonvolatile species B intraparticle diffusion and reaction, with the supply of B coming from region 1. C_{Ae} is the liquid phase concentration of A if for the given bulk partial pressure p_{bA} equilibrium is achieved. C_{Bf} is the average liquid film concentration of B. Bi_{A1}, Bi_{A2}, and Bi_B are the Biot numbers for A and B, respectively, with k_{A1}, k_{A2}, and k_B representing overall mass transfer coefficients that are not, in general, equal.

The Biot numbers Bi_{A1}, Bi_{A2}, and Bi_B are proportional to the overall transport coefficients k_{A1}, k_{A2}, and k_B. k_{A1}, for example, contains contributions from both the gas-to-liquid and liquid-to-solid resistances. k_B contains a contribution from the liquid-side resistance for nonvolatile B. We note that if the criterion of Eq. 2 is violated, the assumption of a uniform concentration in the y direction is not a good one. In order to account for such y-directed gradients the overall transport coefficients must include a contribution from this y-directed intraparticle diffusional resistance. The simplest way is to use a sum of resistances approach. For k_{A1} we have

$$\frac{1}{k_{A1}} = \frac{1}{k_{glA}} + \frac{1}{k_{lsA}} + \frac{\delta_A^*}{D_{Ae}} \tag{8}$$

k_{glA} and k_{lsA} are the gas-to-liquid and liquid-to-solid mass transfer coefficients. The third term approximates the contribution of the intraparticle resistance. The species A effective diffusion length, δ_A^*, is determined as follows.

Intraparticle diffusion and reaction in a catalytic slab of thickness 2δ results in the reactant A concentration profile (y direction)

$$C_{Ay} = (C_{Ay})_s \frac{\cosh(\phi_y y/\delta)}{\cosh(\phi_y)} \tag{9}$$

where $(C_{Ay})_s$ is the A surface concentration. In deriving Eq. 9 we have ignored the x direction (as denoted by the subscript y) and possible depletion of B. We assume that the species A flux into region 1 of the catalyst is approximated by

$$D_{Ae}\left(\frac{dC_{Ay}}{dy}\right)_s = \frac{D_{Ae}}{\delta_A^*}[(C_{Ay})_s - \hat{C}_{Ay}] = k_{A1}^o[C_{Ae} - (C_{Ay})_s] \tag{10}$$

where $1/k_{A1}^o = 1/k_{glA} + 1/k_{lsA}$. The second term resembles the film theory of interphase convective mass transport. In this case, however, the resistance is diffusive, a reaction simultaneously occurs, and $\hat{C}_{Ay}$ is an average concentration over $y \in [0, \delta]$. $\hat{C}_{Ay}$ is determined from Eq. 9 and is given by

$$\hat{C}_{Ay} = (C_{Ay})_s \frac{\tanh(\phi_y)}{\phi_y} \tag{11}$$

Substitution of Eq. 11 in the second term of Eq. 10 and comparison with the first term (using Eq. 9) gives

$$\delta_A^* = \frac{\delta\epsilon}{\phi_y} \tag{12a}$$

where

$$\epsilon = \frac{1}{\tanh(\phi_y)} - \frac{1}{\phi_y} \tag{12b}$$

In the limiting case of an intraparticle diffusion-controlled overall rate ($\phi_y \gg 1$), Eq. 12 simplifies to $\delta_A^* \simeq \delta/\phi_y$. Combining with Eq. 8 gives

$$\frac{1}{k_{A1}} = \frac{1}{k_{A1}^o} + \frac{1}{\sqrt{kD_{Ae}}} \tag{13}$$

In the case of a reaction-controlled overall rate ($\phi_y \ll 1$) the assumption of a uniform concentration in the y direction is a good one and we can ignore the correction for the intraparticle resistance in the y direction. For intermediate cases Eqs. 12a and 12b are used.

The species A overall transport coefficient for the nonwetted part of the catalyst in which reaction occurs, k_{A2}, is analogously given by

$$\frac{1}{k_{A2}} = \frac{1}{k_{gsA}} + \frac{\delta_A^*}{D_{Ae}} \tag{14}$$

where k_{gsA} is the gas-to-solid mass transfer coefficient. The overall transport coefficient for the nonwetted part of the catalyst in

which B is depleted, k_{A3}, is given by Eq. 14 with $\phi_y = 0$, i.e.,

$$k_{A3} = k_{gsA} \tag{15}$$

A similar analysis for the species B overall transport coefficient gives

$$\frac{1}{k_B} = \frac{1}{k_{lsB}} + \frac{\delta_B^*}{D_{Be}} \tag{16}$$

where it can be shown that δ_B^* is identical to δ_A^* (Eq. 12), and k_{lsB} is the species B liquid-to-solid mass transfer coefficient.

In dimensionless form Eqs. 8, 14, 15, and 16 become, using Eq. 12,

$$\frac{1}{Bi_{A1}} = \frac{1}{Bi_{A1}^o} + \frac{1}{\phi}\left[\frac{1}{\tanh(\phi/\alpha)} - \frac{\alpha}{\phi}\right] \tag{17a}$$

$$\frac{1}{Bi_{A2}} = \frac{1}{Bi_{A2}^o} + \frac{1}{\phi}\left[\frac{1}{\tanh(\phi/\alpha)} - \frac{\alpha}{\phi}\right] \tag{17b}$$

$$Bi_{A3} = Bi_{A2}^o \tag{17c}$$

$$\frac{1}{Bi_B} = \frac{1}{Bi_B^o} + \frac{1}{\phi}\left[\frac{1}{\tanh(\phi/\alpha)} - \frac{\alpha}{\phi}\right] \tag{17d}$$

where

$$\frac{1}{Bi_{A1}^o} = \frac{2D_{Ae}}{S}\left(\frac{1}{k_{glA}} + \frac{1}{k_{lsA}}\right) \quad Bi_{A2}^o = \frac{Sk_{gsA}}{2D_{Ae}} \quad Bi_B^o = \frac{Sk_{lsB}}{2D_{Be}} \tag{17e}$$

Inspection of Eqs. 17a, 17b, and 17d reveals that as the active shell thickness gets small ($\alpha \to \infty$) the intraparticle term vanishes, but as it gets large ($\alpha \to 0$) the intraparticle term dominates. These limiting trends are encouraging. Later we provide quantitative evidence that incorporation of the y-directed diffusional resistance into the transport coefficients is a reasonable approximation.

The one-dimensional model with the assumed kinetics has a key feature. Whereas the species A concentration never vanishes, the species B concentration may vanish at some point $s = s^* \le 1$. Whether or not $s^* \le 1$ is determined by the relative liquid film concentrations of A and B (i.e., u_{Bf}) and the relative rates of external transport, intraparticle diffusion, and chemical reaction. From this point on case I represents the case of nondepleting B. Cases II–IV are now described.

If $E_w < s^* < 1$—case II—then a nonwetted region 3 ($s^* < s < 1$) exists in which B is depleted and into which A enters directly from the surrounding gas and diffuses but does not react; i.e.,

$$\frac{d^2u_{A3}}{ds^2} + \alpha Bi_{A3}(1 - u_{A3}) = 0 \tag{18}$$

$$u_{B3} = 0 \tag{19}$$

If $0 < s^* < E_w$—case III—then a wetted region 2 ($s^* < s < E_w$) exists in which B is depleted and A enters from the flowing liquid film. In this case the B that is supplied from the liquid film is converted completely since its supply rate is less than the reaction rate. Species A and B satisfy

$$\frac{d^2u_{A2}}{ds^2} + \alpha Bi_{A1}(1 - u_{A2}) - \frac{\alpha Bi_B u_{Bf}}{m} = 0 \tag{20}$$

$$u_{B2} = 0 \tag{21}$$

The third term in Eq. 20 represents the consumption rate of A by reaction with the entering B, which is completely depleted. In this case, in region 3 ($E_w < s < 1$) species A and B satisfy Eqs. 18 and 19, respectively.

Finally, case IV corresponds to when B depletes completely ($s^* = 0$). In this case there exist two regions: a region 1 ($0 < s < E_w$) in which u_{A1} satisfies Eq. 20, and a region 2 ($E_w < s < 1$) in which u_{A2} satisfies Eq. 18, with $u_{B1} = u_{B2} = 0$.

We should note that the model does not account for diffusive mass transport between the active shell and an inert, permeable core for porous, thin, active surface shell catalysts. Such communication between the wetted and nonwetted parts via the inert core may be important in some cases. This point is considered in more detail in the Discussion section.

The appropriate boundary conditions for case I nondepleting B, are:

At $s = 0$,

$$\frac{du_{A1}}{ds} = 0 \tag{22}$$

$$\frac{du_{B1}}{ds} = 0 \tag{23}$$

At $s = E_w$,

$$u_{A1} = u_{A2} \tag{24}$$

$$u_{B1} = u_{B2} \tag{25}$$

$$\frac{du_{A1}}{ds} = \frac{du_{A2}}{ds} \tag{26}$$

$$\frac{du_{B1}}{ds} = \frac{du_{B2}}{ds} \tag{27}$$

At $s = 1$,

$$\frac{du_{A2}}{ds} = 0 \tag{28}$$

$$\frac{du_{B2}}{ds} = 0 \tag{29}$$

If B depletes in the nonwetted zone (case II; $E_w < s^* < 1$), the boundary conditions include Eqs. 22–27 and

At $s = s^*$,

$$u_{A2} = u_{A3} \tag{30}$$

$$u_{B2} = 0 \tag{31}$$

$$\frac{du_{A2}}{ds} = \frac{du_{A3}}{ds} \tag{32}$$

$$\frac{du_{B2}}{ds} = 0 \tag{33}$$

At $s = 1$,

$$\frac{du_{A3}}{ds} = 0 \tag{34}$$

If B depletes in the wetted zone (case III; $0 < s^* < E_w$) the boundary conditions include Eqs. 22 and 23 at $s = 0$,

At $s = s^*$,

$$u_{A1} = u_{A2} \tag{35}$$

$$u_{B1} = 0 \tag{36}$$

$$\frac{du_{A1}}{ds} = \frac{du_{A2}}{ds} \tag{37}$$

$$\frac{du_{B1}}{ds} = 0 \tag{38}$$

At $s = E_w$,

$$u_{A2} = u_{A3} \tag{39}$$

$$\frac{du_{A2}}{ds} = \frac{du_{A3}}{ds} \tag{40}$$

and Eq. 34 at $s = 1$.

Finally, if B depletes completely (case IV; $s^* = 0$) the boundary conditions include the no-flux conditions, Eqs. 22 and 28, and continuity, Eqs. 39 and 40.

In Appendix 1 the general solutions are provided for the four possible cases; case I (nondepleting B), case II (B depletion in nonwetted zone), case III (B depletion in wetted zone), and case IV (complete B depletion). Definitions of terms are also provided.

If B does not deplete, Eqs. 1.A–1.D in Appendix 1 and eight boundary conditions, Eqs. 22–29, are applied to determine the eight integration constants. In this case the solution for species A is independent of species B. After some algebraic manipulation we obtain expressions for K_1–K_8; these are provided in Appendix 2.

If B depletes in the nonwetted zone, Eqs. 1.A–1.F in Appendix 1 and eleven boundary conditions, Eqs. 22–27 and 30–34, are used to determine the ten integration constants and s^*, the point of B depletion. After some cumbersome algebra, we obtain expressions for K_1–K_{10}, some of which are in terms of s^*. The remaining expression is a rather lengthy implicit function of s^*, $F(s^*, E_w, p) = 0$, where p is a vector of model parameters. Appendix 3 shows the expression for K_1–K_{10} and $F(s^*, E_w, p) = 0$. $F(s^*, E_w)$ is independent of the integration constants upon substitution of expressions for K_2, K_5, K_6, and K_7, which are in terms of s^*.

Similarly, if B depletes in the wetted zone, Eqs. 1.A, 1.B, and 1.G–1.J in Appendix 1 and nine boundary conditions, Eqs. 22, 23, 28, and 35–40, are used to determine the eight integration constants and s^*. Again, some algebra gives K_1–K_6, K_9, K_{10}, and a function of s^*, $F(s^*, E_w, p) = 0$; these are provided in Appendix 4.

In the case of complete B depletion there are four constants, K_5, K_6, K_9, and K_{10}, of which K_5 and K_9 are zero. K_6 and K_9 are simply found and are not shown.

Concentration Profile Features

It is instructive to examine the influence of the dimensionless model parameters (E_w, αBi_{A1}, αBi_{A2}, αBi_B, u_{Bf}, ϕ, and m) on the qualitative features of the dissolved gas (A) and liquid (B) reactant concentration profiles. For the moment we neglect any influence of y-directed diffusional limitations; i.e., the overall transport coefficients are not adjusted for changes in ϕ and α. However, the results are applicable for all cases by using Eqs. 17a–17e.

Figure 2a corresponds to a base case in which $E_w = 0.3$, $\alpha Bi_{A1} = 1$, $\alpha Bi_{A2} = 100$, $\alpha Bi_B = 100$, $u_{Bf} = 20$, $\phi = 50$, and $m = 1$. For the remaining cases, Figures 2b–2n, a single parameter is changed while the others are held fixed. For example, Figures 2a–2b together exhibit the effect of E_w on the A and B profiles. Remaining pairs of figures (Figures 2c–2d, 2e–2f, etc.) show how the base case profiles are affected by a significant increase and decrease in each parameter. In each case a vertical dashed line denotes the wetting efficiency E_w. Another dashed line denotes s^*, the point of B depletion (if depletion occurs).

The base case, Figure 2a, typifies a reaction that is limited by external mass transfer and intraparticle diffusion and for which transport of A on the nonwetted part is significantly more effective than on the wetted part; i.e., $\alpha Bi_{A2} = 100\alpha Bi_{A1}$. The concentration of B decreases from its maximum value at the center of region 1 to zero at $s^* = 0.78$. The decrease is more pronounced in region 2 since B is only supplied in region 1. On the other hand, A decreases from its maximum value at the center of the nonwetted part to a level very close to zero within region 1. Thus, A and B diffuse in opposite directions while reacting. The stepwise decrease in A from $s = 1$ to $s = 0$ is a result of the discontinuous kinetics at $s = s^*$, Eq. 1, and the discontinuous external transport rate at $s = E_w$. Except near the interfacial zones between regions 1 and 2 and regions 2 and 3, the A profile is almost flat. This indicates that the reaction is sufficiently fast that any A supplied by external transport reacts instantaneously

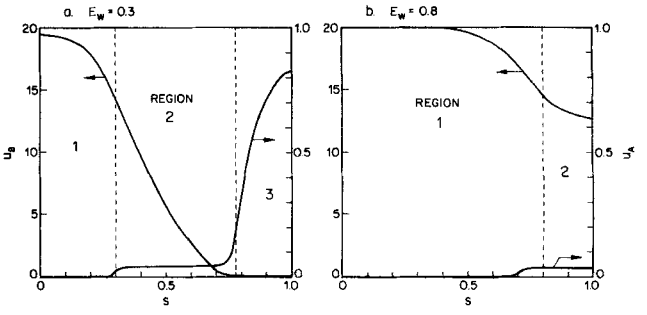

Figure 2a, b. Species A and B concentration profiles.
a. Base case: $\alpha Bi_{A1} = 1$; $\alpha Bi_{A2} = 100$; $\alpha Bi_B = 100$; $\phi = 100$; $m = 1$; $u_{BF} = 20$; $E_w = 0.3$
b. Influence of E_w change.

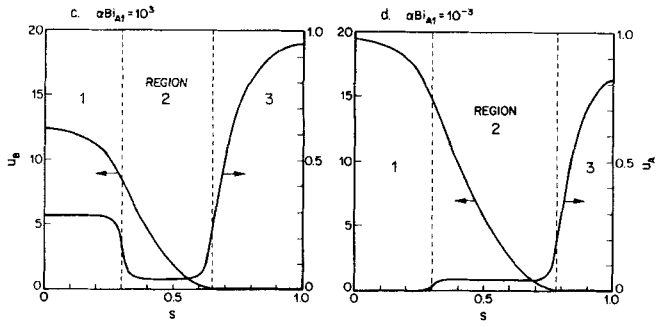

Figure 2c, d. Influence of αBi_{A1} on A and B concentration profiles.

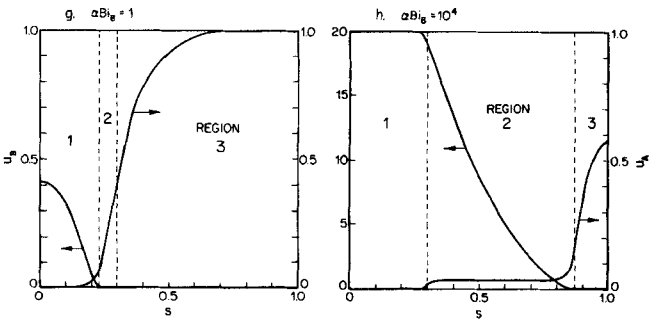

Figure 2g, h. Influence of αBi_B on A and B concentration profiles.

with B. In fact, inspection of Eqs. 3 and 5 reveals that for $\phi \gg 1$

$$u_{A1} \cong \frac{\alpha Bi_{A1}}{\alpha Bi_{A1} + \phi^2} \tag{41}$$

$$u_{A2} \cong \frac{\alpha Bi_{A2}}{\alpha Bi_{A2} + \phi^2} \tag{42}$$

as long as the widths of region 1 (E_w) and region 2 ($s^* - E_w$) are not too small.

If the wetting efficiency is increased to 0.8, Figure 2b, the supply of B is sufficient to prevent its depletion. Note also that most of A which enters the wetted part reacts in region 1 since the supply rate is much smaller than the chemical reaction rate.

The influence of αBi_{A1} is exhibited in Figure 2c ($\alpha Bi_{A1} = 10^3$) and Figure 2d ($\alpha Bi_{A1} = 10^{-3}$). For the case of Figure 2c a more effective transport rate of the gaseous reactant through the wetted part than the nonwetted part corresponds to the situation for which the liquid film contains a high concentration of the dissolved gaseous reactant and the surrounding gas is comprised essentially of an inert. Thus, the A profile is nonmonotonic, with its minimum concentration occurring within region 2. Not surprisingly, the more effective A transport in region 1 decreases B appreciably as compared to region 1 for the case of Figure 2a. Figure 2d is almost identical to Figure 2a, indicating that a decrease in αBi_{A1} from 1 to 10^{-3} has little effect; i.e., the A that reacts is essentially all supplied from the nonwetted part in both cases.

The influence of αBi_{A2} is demonstrated in Figure 2e ($\alpha Bi_{A2} = 10$) and Figure 2f ($\alpha Bi_{A2} = 10^4$). The case of Figure 2e shows that under external mass-transfer controlled conditions and negligible difference in the mass transfer coefficients for A in the nonwetted and wetted parts, the A profile is essentially zero throughout regions 1 and 2. Since B does not deplete, there is not a large increase in A due to the presence of a depleted liquid reactant zone as in Figure 2a. For very rapid transport of A in the nonwetted part species B is depleted very close to the edge of the supply zone, Figure 2f. A increases rapidly from its limiting value in region 1, Eq. 41, to near unity at $s = 0.4$, Eq. 1.E.

The influence of αBi_B is examined in Figure 2g ($\alpha Bi_B = 1$) and Figure 2h ($\alpha Bi_B = 10^4$). The ineffective supply rate of B from the liquid in the case of Figure 2g dramatically lowers the B concentration at all points, with the depletion point occurring within the wetted region. The A profile in region 2 satisfies Eq. 1.G in Appendix 1. An increase in αBi_B to 10^4, Figure 2h, serves to maintain u_{B1} at essentially its maximum level of $u_{Bf} = 20$ within region 1. The reaction and supply of A are sufficiently fast, however, to deplete B in the nonwetted zone.

The influence of the Thiele modulus ϕ is exhibited in Figure 2i ($\phi = 150$) and Figure 2j ($\phi = 5$). In comparing the case of Figure 2i to that of Figure 2a, it is evident that the increased catalytic activity reduces the concentration of A in region 1 and that B depletes closer to the wetted part. A much slower reaction, Figure 2j, results in a reaction-controlled overall rate. In this case B does not deplete and both the A and B profiles are much smoother than under transport-controlled conditions.

The influence of m is depicted in Figure 2k ($m = 10$) and Figure 21 ($m = 0.1$). A variation in m amounts to an alteration in the stoichiometric ratio with all other conditions fixed. As expected, for $m = 10$ as compared to $m = 1$, Figure 2a, B depletes much closer to region 1. A two-order of magnitude

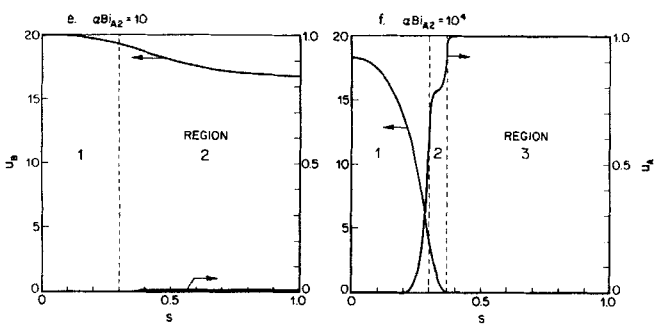

Figure 2e, f. Influence of αBi_{A2} on A and B concentration profiles.

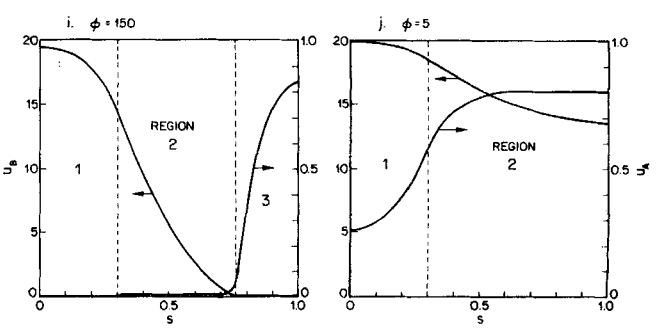

Figure 2i, j. Influence of ϕ on A and B concentration profiles.

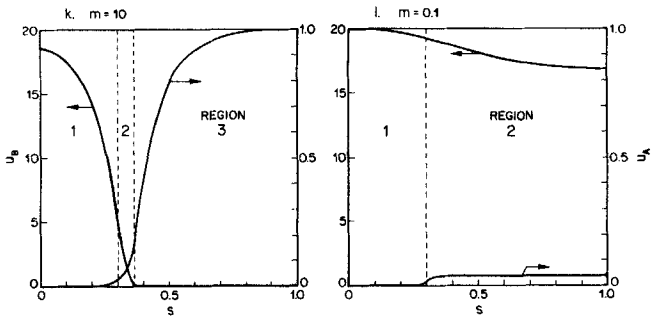

Figure 2k, l. Influence of m on A and B concentration profiles.

decrease to 0.1, Figure 2e, significantly increases the concentration of B at all points within the pellet.

Finally, the influence of the ratio of the concentration of B in the film to the equilibrium concentration of A is illustrated in Figure 2m ($u_{BF} = 100$) and Figure 2n ($u_{Bf} = 0.25$). As expected, an increase (decrease) in u_{Bf} increases (decreases) B at all points in the pellet.

Catalyst Effectiveness as a Function of Wetting Efficiency

The features of the several interacting rate processes are best investigated by computing the overall catalyst effectiveness η as a function of the model parameters. The effectiveness is defined as the ratio of the overall rate per unit catalyst volume to the rate with complete wetting ($E_w = 1$), no external or intraparticle transport limitations, and no liquid reactant depletion. The overall rate is given by

$$r = \eta k C_{Ae}(V_{p,\text{act}}/V_p) \tag{43}$$

where $V_{p,\text{act}}(V_p)$ is the active zone (total pellet) volume. For case I, no B depletion, $s^* > 1$ and

$$\eta = \frac{1}{\phi^2}\left[\alpha Bi_{A1}\left(E_w - \int_0^{E_w} u_{A1}\,ds\right) + \alpha Bi_{A2}\left(1 - E_w - \int_{E_w}^{1} u_{A2}\,ds\right)\right] \tag{44}$$

where the first integral is given in Appendix 5 by Eq. 5.A and the second by Eq. 5.B with $s^* = 1$. Expressions for the constants are provided in Appendix 2.

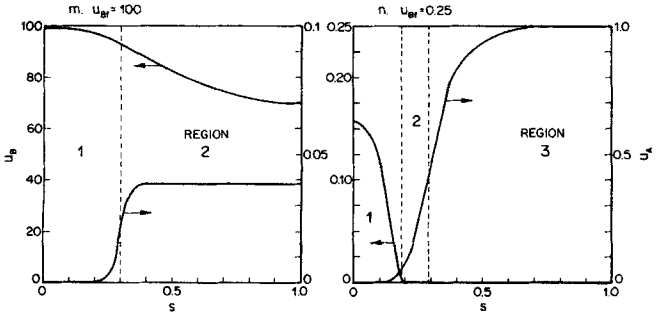

Figure 2m, n. Influence of u_{Bf} on A and B concentration profiles.

For case II, B depletion in the nonwetted part,

$$\eta = \frac{1}{\phi^2}\left[\alpha Bi_{A1}\left(E_w - \int_0^{E_w} u_{A1}\,ds\right) + \alpha Bi_{A2}\left(s^* - E_w - \int_{E_w}^{s^*} u_{A2}\,ds\right) + \alpha Bi_{A3}\left(1 - s^* - \int_{s^*}^{1} u_{A3}\,ds\right)\right] \tag{45}$$

where the three integrals are given in Appendix 5. For case III, B depletion in the wetted part,

$$\eta = \frac{1}{\phi^2}\left[\alpha Bi_{A1}\left(E_w - \int_0^{s^*} u_{A1}\,ds - \int_{s^*}^{E_w} u_{A2}\,ds\right) + \alpha Bi_{A3}\left(1 - E_w - \int_{E_w}^{1} u_{A3}\,ds\right)\right] \tag{46}$$

where the three integrals are given in Appendix 5. For each case of depleting B, s^* is the feasible root of $F(s^*, E_w) = 0$ ($E_w < s^* \le 1$ for case II, $0 < s^* < E_w$ for case III) using expressions for the constants in Appendices 3 and 4.

Before proceeding with the effectiveness simulations for the partially wetted catalyst we will check the limiting case of a completely wetted catalyst with no liquid reactant depletion. In this case, application of the no-flux boundary conditions at $s = 0$ and $S/2$ to Eq. 1.A gives the flat A profile described by Eq. 41. The effectiveness is equal to u_{A1}, and after combining with Eq. 43 and rearranging gives an overall rate expression

$$r = \left(\frac{1}{1/k + \delta/k_{A1}}\right) C_{Ae} V_{p,\text{act}}/V_p \tag{47}$$

Equation 47 is virtually identical to the result for the overall rate of a first-order reaction on a nonporous catalyst of volume V_p and external surface area S_x with an external mass transfer coefficient k_{A1}. The only difference is that δ has replaced $V_{p,\text{act}}/S_x$. This is not surprising since our model in the case of a very thin surface shell (i.e., no y-directed diffusional limitations) is essentially that of a surface-active catalyst. For the uniformly active catalyst, k_{A1} is given by Eqs. 8 and 12. Upon substitution of these into Eq. 47 we can compare the result to the well-known overall rate expression for a first-order reaction in a completely wetted catalytic slab of thickness 2δ in which there are external transport limitations and severe intraparticle diffusional limitations (Froment and Bischoff, 1979); i.e.,

$$r = \left[\frac{1}{\dfrac{\delta}{\sqrt{kD_{Ae}}} + \delta\left(\dfrac{1}{k_{glA}} + \dfrac{1}{k_{lsA}}\right)}\right] C_{Ae} \tag{48}$$

Our model gives for $\phi_y \gg 1$

$$r = \left[\frac{1}{\dfrac{1}{k} + \dfrac{\delta}{\sqrt{kD_{Ae}}} + \delta\left(\dfrac{1}{k_{glA}} + \dfrac{1}{k_{lsA}}\right)}\right] C_{Ae} \tag{49}$$

The only difference is the $1/k$ term in the denominator, which for $\phi_y \gg 1$ is negligible.

The influence of each parameter on η will be examined in the same manner as the concentration profiles. A base case is selected corresponding to $\alpha Bi_{A1} = 1$, $\alpha Bi_{A2} = 100$, $\alpha Bi_B = 100$, $u_{Bf} = 20$, $\phi = 50$, and $m = 1$. A family of η vs. E_w curves is computed for several values of one of the parameters while fixing the other parameters. The transport coefficients are not adjusted for diffusional limitations in the y direction, although the results are general if one uses Eqs. 17a–17e. The impact of these limitations is considered later.

The influence of αBi_{A1} is demonstrated in Figure 3. On each curve the circle denotes the critical wetting efficiency, E_w^*, which gives $s^* = 1$; i.e., for $E_w > E_w^*$ B does not deplete but for $E_w < E_w^*$ B depletes for some $s^* \in (E_w, 1)$. A curve with no circle implies that B does not deplete for any E_w. Although impossible to show in a semilogarithmic plot, all the curves satisfy $\eta(E_w \to 0) \to 0$, implying that in the limit of no wettng, no reaction occurs since B is not supplied. Surprisingly, previous models have not satisfied this obvious condition.

For $\alpha Bi_{A1} > \alpha Bi_{A2}$ (= 100) η is an increasing function of E_w. This suggests that when the liquid film is the dominant supply source of A, an increase in wetting is always accompanied by a rate increase. Note that E_w^* approaches unity as αBi_{A1} becomes unbounded. This indicates that the increasingly effective supply of A through the liquid film causes B to deplete even for a very thin nonwetted zone.

When αBi_{A1} is less than αBi_{A2} (= 100) η attains a maximum at an intermediate E_w, which we denote by E_w^m. A maximum in η is a result of two counteracting effects. To the left of the maximum an increase in η with E_w results from an increasing catalyst utilization. By catalyst utilization we refer to the length of reaction zone s^* in which B is not depleted and in which the reaction takes place. s^* always exceeds η since the rate is zero in the depleted zone of dimensionless length $1 - s^*$. Note that for the $\alpha Bi_{A1} = 50$ and 1 curves, E_w^* is nearly equal to E_w^m. This shows

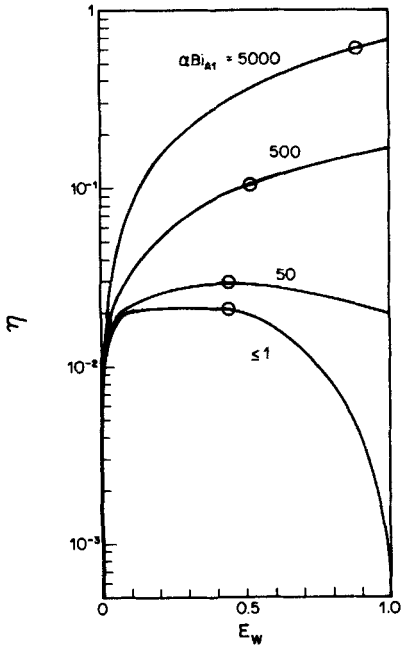

Figure 3. Influence of αBi_{A1} on effectiveness vs. wetting efficiency.

Other parameter values as in Figure 2a.

that when the wetting is sufficient to supply B throughout the pellet another effect takes over that reduces η with further increases in E_w. This second effect is caused by the less effective transport of A on the wetted part compared to the nonwetted part.

When αBi_{A1} is sufficiently small compared to αBi_{A2} (<1), A is supplied almost entirely from the nonwetted part and there is no detectable influence of αBi_{A1} on η. In this limiting case η decreases precipitously as complete wetting is approached. This decrease is due to a negligible supply rate of A as $E_w \to 1$ and is analogous to the negligible supply rate of B as $E_w \to 0$.

Finally, note that the bottom curve corresponding to small αBi_{A1} has a rather flat maximum, implying that the effectiveness is essentially independent of E_w in this range. In this case a wetting increase serves to increase the catalyst utilization s^*, however, this has little effect on the effectiveness. To be more concise, consider an alternative expression for η given by

$$\eta = \int_0^{E_w} u_{A1}\, ds + \int_{E_w}^{s^*} u_{A2}\, ds. \tag{50}$$

It is also useful to refer to the concentration profiles in Figure 2d where $\alpha Bi_{A1} = 10^{-3}$. Since ϕ is large, u_{A1} and u_{A2} are approximately constants and are given by Eqs. 41 and 42, respectively. Using Eq. 50, η is therefore approximated by

$$\eta = (u_{A1} - u_{A2})E_w + u_{A2}s^* \tag{51}$$

Since $\alpha Bi_{A2} \gg \alpha Bi_{A1}$, we have $u_{A2} \gg u_{A1}$ and $\eta \simeq (s^* - E_w)u_{A2}$. Thus, within the flat region of η, an increase in E_w increases s^* proportionally. In physical terms, most of A that reacts enters from the nonwetted part. An increase in wetting maintains the concentration of B at the wetted-nonwetted interface at essentially its maximum value u_{Bf}, as little of it is consumed in region 1 due to the ineffective supply rate of A through the liquid film. As a result, the major reaction zone, region 2, maintains an almost constant width as E_w increases since the slow diffusion of A and B prevents additional reaction. Thus, the intraparticle diffusion of A and B is the controlling rate process. As s^* approaches unity, however, the external transport of A becomes the limiting process and η declines.

The influence of αBi_{A2} on the η vs. E_w dependence is demonstrated in Figure 4. The family of curves intersect at $E_w = 1$ because a variation in αBi_{A2}, the Biot number for the nonwetted zone, simply does not have any effect on a completely wetted catalyst pellet. Similar to Figure 3, all the curves satisfy $\eta(E_w \to 0) \to 0$ although this cannot be shown on a semilogarithmic plot.

As αBi_{A2} is increased above αBi_{A1} a maximum in the effectiveness is predicted. The E_w giving the maximum, E_w^m, increases from near zero for $\alpha Bi_{A2} \to 1$ to near unity as αBi_{A2} becomes unbounded. The maximum flattens appreciably as αBi_{A2} increases. Similarly, the E_w above which B does not deplete, E_w^*, increases from near zero to near unity. Again, a maximum is attained as E_w increases because of the counteracting effects of an increasing catalyst utilization and a decreasing supply rate of A. Within the E_w range in which η is insensitive we again have, using Eqs. 41, 42, and 51, the approximation that $\eta \simeq (s^* - E_w)u_{A2}$. As $\alpha Bi_{A2} \to \infty$, η is essentially constant over a wide E_w range, demonstrating again the regime of intraparticle diffusion control.

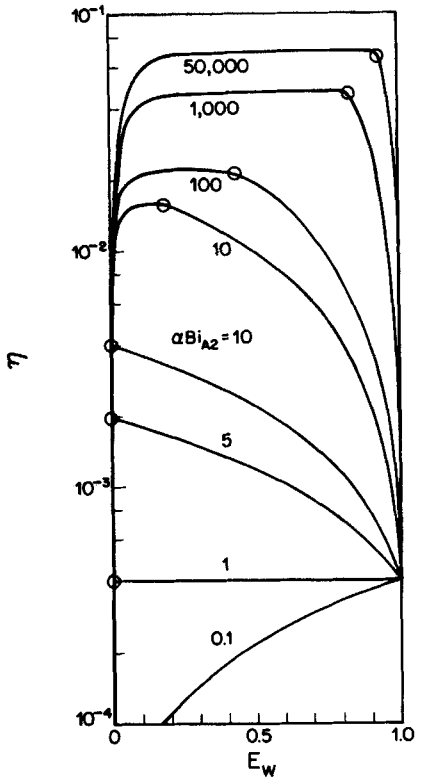

Figure 4. Influence of αBi_{A2} on effectiveness vs. wetting efficiency.
Other parameter values as in Figure 2a.

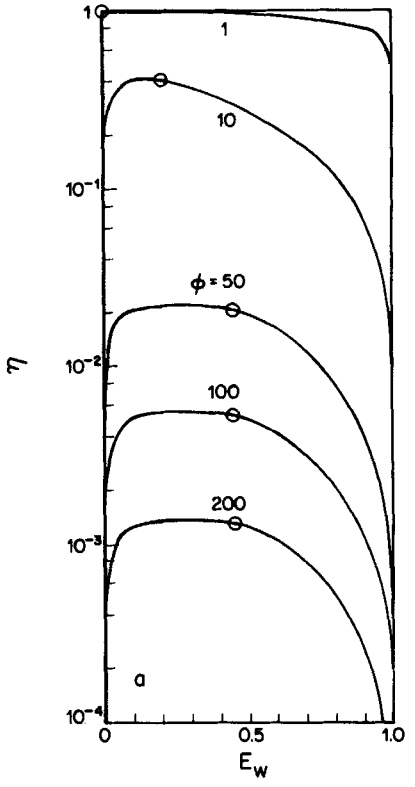

Figure 5a. Influence of ϕ on effectiveness vs. wetting efficiency.
Other parameter values as in Figure 2a.

The influence of the Thiele modulus on the η vs. E_w dependence is demonstrated in Figure 5a. As expected, an increase in ϕ decreases the effectiveness at all wetting levels. In the limit of $\phi \to 0$—a reaction-controlled overall rate—$\eta = 1$ for all E_w except for $E_w \to 0$, at which point the supply of B is negligible. Each curve exhibits a maximum since $\alpha Bi_{A2} > \alpha Bi_{A1}$. An interesting result is that as ϕ is increased from 1 to 10 the E_w range in which η is relatively constant decreases. As ϕ is further increased this range proceeds to increase until it attains a constant value ($E_w = 0.2$ to 0.4) for $\phi > 50$. These predictions are explained as follows.

As ϕ increases from 1 to 10 a shift from reaction control ($\eta \simeq 1$) to external transport control occurs, resulting in the characteristic influence of the difference in transport coefficients for A. The maximum is rather sharp at $\phi = 10$ since complete catalyst utilization is attained for a small wetting level ($E_w^* \simeq 0.2$). For $E_w > E_w^*$ the ineffective transport of A in the wetted zone causes a sharp η decrease.

As ϕ is increased to 50 and higher the maximum in η is almost constant over a wide E_w range. This insensitivity is a result of intraparticle diffusion control as explained above. However, increases in ϕ above 50 do not increase the E_w range in which η is constant. This is a result of the transport of A becoming the controlling process as ϕ becomes unbounded. This fact is demonstrated clearly by examining how s^* depends on E_w, Figure 5b. When the reaction is slow ($\phi \to 0$) very small wetting levels are sufficient to supply B throughout the entire pellet, noting that $E_w^*(\phi \to 0) \to 0$. As ϕ is increased a higher wetting efficiency is required to attain the same level of utilization or to utilize completely the pellet. However, Figure 5b shows that the s^* vs. E_w curves compress into essentially a single curve as ϕ becomes unbounded. This implies that despite the increasingly rapid reaction, species B cannot be depleted any closer to the wetted zone since the supply rate of A in the nonwetted zone is insufficient to further deplete B.

In Figures 6, 7, and 8 we examine the three key parameters involving the liquid reactant B; namely, αBi_B, m, and u_{Bf}. The

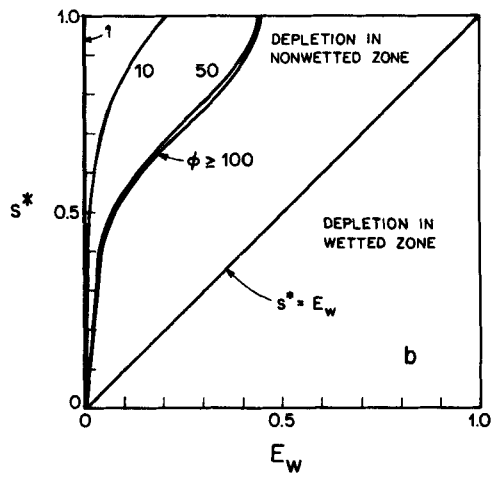

Figure 5b. Dependence of catalyst utilization s^* on wetting efficiency for several ϕ values.

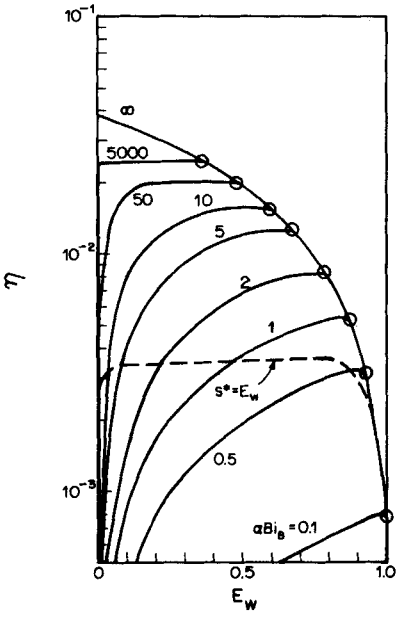

Figure 6. Influence of αBi_B on effectiveness vs. wetting efficiency.
Other parameter values as in Figure 2a.

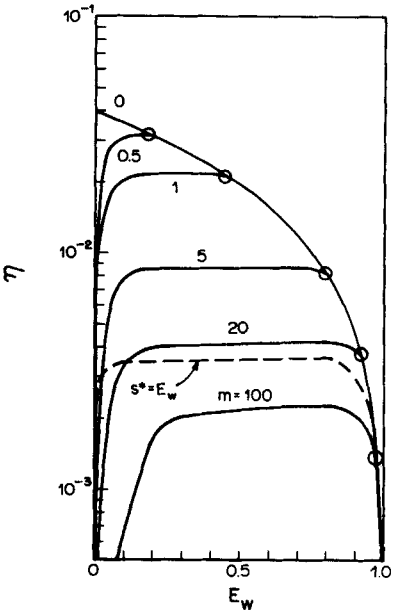

Figure 8. Influence of m on effectiveness vs. wetting efficiency.
Other parameter values as in Figure 2a.

influence of these parameters on the η vs. E_w dependence is qualitatively the same. This is because an increase (decrease) in αBi_B (overall mass transfer coefficient for B) or u_{Bf} (the concentration of B in the film) or a decrease (increase) in m (the stoichiometric ratio) serves to increase (decrease) the total amount of unconverted B within the pellet. The zero-order dependence on B in the kinetic rate expression is clearly conveyed as αBi_B, u_{Bf}, and m^{-1} become unbounded or approach zero. In the former case, unless the reaction rate and supply rate of A are sufficiently large, B will not deplete and the effectiveness is completely independent of B. Computation of η vs. E_w then utilizes the nondepleted solution (case I; Eqns. 1.A–1.D in Appendix 1). In the latter case, unless the reaction rate and supply rate of A are sufficiently small, B will deplete within the wetted zone and the case III solution applies (Eqs. 1.A, 1.B, 1.G–1.J, and Appendix 4).

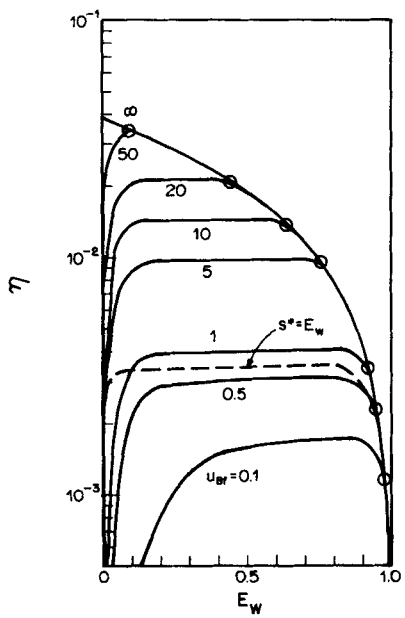

Figure 7. Influence of u_{Bf} on effectiveness vs. wetting efficiency.
Other parameter values as in Figure 2a.

The nondepleted B solution ($\alpha Bi_A = 1$, $\alpha Bi_A = 100$, and $\phi = 50$) is plotted in Figures 6, 7, and 8 and is labeled as $\alpha Bi_A \to \infty$, $u_{Bf} \to \infty$, and $m \to 0$, respectively. This solution intersects $E_w = 0$ and $E_w = 1$ in each case and is a monotonic decreasing function of E_w. Note that this limiting solution has no physical meaning at $E_w = 0$ and provides no means of satisfying $\eta(E_w \to 0) \to 0$. However, the solution serves as an upper bound on η for all αBi_B, u_{Bf}, and m at a fixed E_w.

The demarcation between B depletion in the wetted zone and the nonwetted zone (i.e., $s^* = E_w$) is plotted as the dashed locus in Figures 6–8. The intersection of any η vs. E_w curve with this locus gives the wetting efficiency below which depletion occurs in the wetted zone. Below this locus the overall rate is clearly limited by the B supply rate. As expected, as the total amount of B decreases (i.e., as αBi_B, u_{Bf}, m^{-1} decrease) this critical wetting efficiency increases. For example, for $\alpha Bi_B = 0.5$, B depletes within the wetted zone for all E_w less than 0.85.

The families of η vs. E_w curves form interesting and qualitatively identical patterns as either αBi_B, u_{Bf}, or m is varied. For each family, besides being bounded by the nondepleted solution, the broadness of the effectiveness maximum switches from being vary narrow, to broad, and then back to narrow as αBi_B, u_{Bf}, and m^{-1} decrease. The sharp maximum near the upper bounding solution (large supply of B) demonstrates the detrimental impact of the ineffective supply of A on the wetted part on the effectiveness even for very small wetting efficiencies. As the supply of B is decreased an intermediate αBi_B, u_{Bf}, or m^{-1} range is encountered in which intraparticle diffusion is the con-

trolling rate process, as indicated by the flat maximum. Further decreases in αBi_B, u_{Bf}, and m^{-1} result in the B supply rate becoming the limiting process. This is indicated by the sharp effectiveness maximum; i.e., the switch from a B supply rate-limiting regime to an A supply rate-limiting regime occurs in a narrow wetting efficiency range.

Criterion for Depletion of Liquid Reactant

The model predicts that when the transport is more effective on the nonwetted than on the wetted part ($\alpha Bi_{A2} > \alpha Bi_{A1}$), the effectiveness achieves a maximum at an intermediate wetting efficiency E_w^m. In many of the cases E_w^m corresponds closely with the wetting efficiency below which initiation of liquid reactant depletion at $s = 1$ occurs, E_w^*. For this reason, it is convenient to compute the conditions resulting in the onset of B depletion. To do this we have the condition

$$F(s^* = 1, E_w, p) = 0 \tag{52}$$

which must be solved for one of the model parameters. We decided to compute the critical Thiele modulus above which B depletion occurs, ϕ^*, as a function of E_w. This gives the minimal catalytic activity necessary to initiate depletion of the liquid reactant for a given set of conditions (since k is contained only in ϕ). Moreover, determination of ϕ^* enables one to check the validity of the common assumption in the literature that the liquid reactant is in excess throughout the entire pellet. In this calculation we have not included the contribution by the intraparticle resistance in the y direction. To do so merely requires an incorporation of Eqs. 17a–17e into Eq. 52.

Figure 9 shows the model predictions of ϕ^* vs. E_w for several u_{Bf} values with the other parameters assuming their base case values. Several points should be noted. First, ϕ^* is a monotonic increasing function of E_w. This means that as E_w increases the activity necessary to deplete B increases. Second, for a sufficiently large E_w, ϕ^* becomes unbounded. This implies that if the wetted zone and hence overall B supply rate is sufficiently large, then it is virtually impossible to deplete B. Under these conditions the supply rate of A is the controlling process. This follows the result discussed earlier in relation to Figure 5b. An increase in αBi_{A1} or αBi_{A2} in Figure 9 would move the steep portions of the curves closer to $E_w = 1$ since this would increase the A supply rate. Third, for a fixed E_w an increase in u_{Bf} requires an increasingly active catalyst to deplete B. A similar trend is obtained from an increase in αBi_B or m^{-1}.

Impact of Intraparticle Diffusion in the y Direction

In this section we distinguish between the external resistance and y-directed intraparticle resistance contributions to the modified overall transport coefficients, Eqs. 17a–17e. Our objective is to focus on the influence of the diffusional resistance in the y direction. We define a new base case: $\alpha Bi^o_{A1} = 1$, $\alpha Bi^o_{A2} = 100$, $\alpha Bi^o_B = 100$, $u_{Bf} = 20$, $m = 1$, and $\alpha = 5$. Figure 10 shows the dependence of the effectiveness on the wetting efficiency for the base case (solid line) for several values of the Thiele modulus. For comparison we include the model predictions if the y-directed diffusional limitations are ignored, using the previous base case values (dashed line), i.e., $\alpha Bi_{A1} = 1$, $\alpha Bi_{A2} = 100$, $\alpha Bi_B = 100$, $u_{Bf} = 20$, and $m = 1$. For a sufficiently slow reaction ($\phi \to 0$) and/or thin active layer ($\alpha \gg 1$) the approximation of a uniform concentration in the y direction is a good one. Under these conditions the effectiveness predictions for each case are nearly identical. We have selected the new base case transport coefficient values so that when the y-directed intraparticle contribution is insignificant compared to the external contribution,

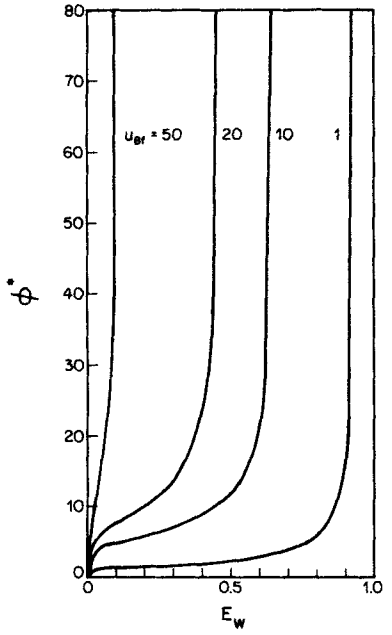

Figure 9. Dependence of minimum Thiele modulus necessary to deplete B at $s = 1$ as a function of wetting efficiency.
Other parameter values as in Figure 2a.

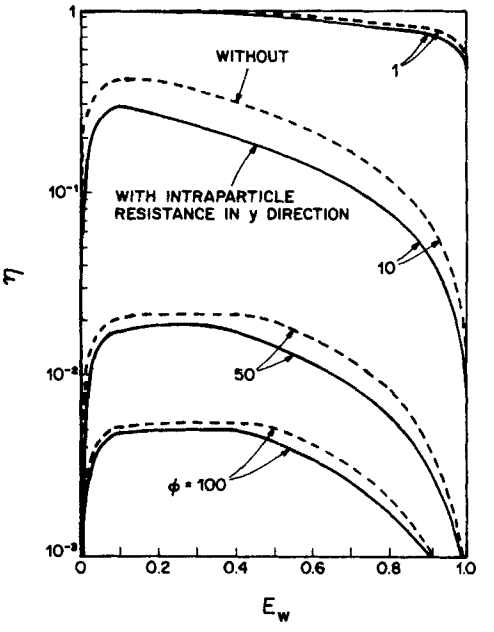

Figure 10. Dependence of effectiveness on wetting efficiency with Thiele modulus as a parameter.
Difference between —— and - - - shows impact of intraparticle diffusion in y direction.

using Eqs. 17a–17e, we have $Bi_{A1} = Bi^{o}_{A1}$, $Bi_{A2} = Bi^{o}_{A2}$, and $Bi_B = Bi^{o}_B$. Figure 10 shows the close agreement when $\phi = 1$.

As ϕ is increased we can directly check the impact of the diffusional resistance in the y direction by comparing the predictions of the two cases. Even without y-directed diffusional limitations, η decreases as ϕ increases, as in Figure 5a, because of intraparticle limitations in the x direction and external resistances. By including the additional diffusional resistance there is an additional η decrease for a given ϕ. This decrease is especially apparent for intermediate values of ϕ. For example, for $\phi = 10$, $\eta(E_w = 0.2)$ decreases from 0.32 to 0.17, a 47% decrease.

For the example selected, when ϕ is sufficiently large the additional resistance does not significantly affect the effectiveness. This minor impact is a result of the external transport of A being the dominant controlling process. This is conveniently shown for the case of a completely wetted pellet without B depletion. Without y-directed diffusional limitations we have, using Eq. 47, the exact result

$$\eta = \frac{\alpha Bi_{A1}}{\alpha Bi_{A1} + \phi^2} \tag{53}$$

With the y-directed diffusional limitations Eq. 17a is substituted into Eq. 53, giving

$$\eta = \frac{\alpha Bi^{o}_{A1}}{(\alpha + \epsilon\phi)Bi^{o}_{A1} + \phi^2} \tag{54}$$

For $\phi \gg 1$ the two cases give similar results, since $\phi \gg \alpha$, $\epsilon \cong 1$, and $Bi_{A1} = Bi^{o}_{A1} \ll \phi$. Although not as straightforwardly shown, the same reasoning applies to the partially wetted pellet with severe external transport limited conditions; i.e., the additional intraparticle resistance has little effect.

On the other hand, if external transport is more effective the impact of the y-directed diffusion may be significant. To show this, we consider again the completely wetted pellet. Figure 11 shows the dependence of the effectiveness on the aspect ratio α for the case in which the y-directed diffusion is ignored (dashed lines; Eq. 53) and is accounted for (solid lines; Eq. 54) using $Bi_{A1} = Bi^{o}_{A1} = 100$ and three different values of ϕ. The results show that the two cases predict identical η values as $\alpha \to \infty$; i.e., the active shell is so thin that y-directed gradients do not exist. However, for bounded α and intermediate ϕ values the discrepancy in the effectiveness predictions is large. Under these conditions the intraparticle diffusion is a key rate process. A similar conclusion can be drawn by examining the $\phi = 10$ curves in Figure 10.

In order to quantitatively check the validity of incorporating the y-directed intraparticle diffusional resistance into an overall transport coefficient, we can compare our model to the exact predictions of Ramachandran and Smith (1979). They used a finite-difference technique to solve the two-dimensional reaction and diffusion model of a partially wetted catalyst of rectangular cross section. They assumed an infinite supply of the nonvolatile liquid reactant. As long as the same aspect ratio (α) is used, our nondepleted B model is identical to theirs except for our approximate accounting for the intraparticle diffusion in the y direction.

We used identical values given by Ramachandran and Smith in computing the effectiveness as a function of the wetting efficiency ($\phi = 7.5$ and 21.3, $Bi^{o}_{A1} = 5$, $Bi^{o}_{A2} = 50$, and $\alpha = 1$, using our notation). Figure 12 compares our model predictions with their exact values. The trends are identical. The one-dimensional model predictions are within 15% of the exact values. This excellent agreement is obtained despite stretching our model's geometric applicability in letting the aspect ratio α equal unity. We expect that for $\alpha > 5$ the agreement would be even better. Most important, the agreement indicates the success of the one-dimensional model in qualitatively predicting the performance of uniformly active catalysts.

Analysis of Experimental Data

In this section we demonstrate the ability of the model to predict a set of experimental rate data in which partial wetting played a key role. The study (Herskowitz et al., 1979) employed palladium on alumina catalyzed α-methylstyrene (AMS) hydrogenation as the test reaction. The kinetics of this reaction have been shown in this study and in other studies (Morita and Smith, 1978; El Hisnawi et al., 1982) to be first- (zero-) order with respect to hydrogen (AMS); consequently, our model can be used. It should be pointed out, however, that other investiga-

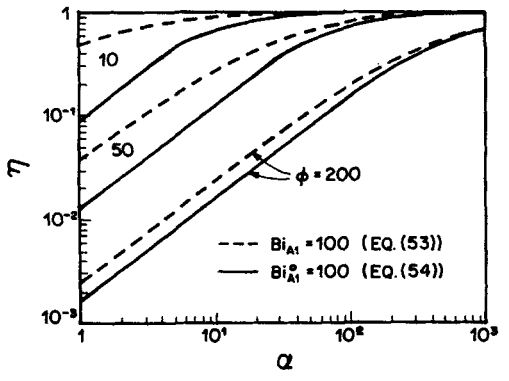

Figure 11. Dependence of effectiveness on aspect ratio α for fully wetted pellet.

Difference between —— and - - - shows impact of intraparticle diffusion in y direction.

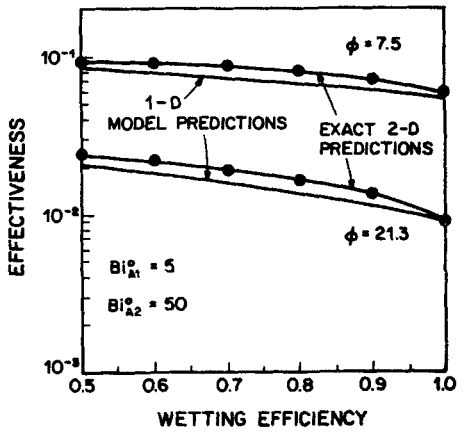

Figure 12. Comparison of model predictions and exact 2-D predictions of Ramachandran and Smith (1979).

$\alpha = 1$; Bi and ϕ, values as shown

tors have reported a nonzero-order dependence with respect to AMS under conditions in which AMS is not in large excess (Babcock et al., 1957; Turek and Lange, 1981). We emphasize that the following data analysis is not intended to be an accurate data fit but is intended to provide some physical insight.

Herskowitz et al. used a 0.0254 m ID differentially operated trickle-bed reactor in their study. Figure 13 shows the measured dependence of the global reactor rate on the total flow rate of the feed liquid containing an equilibrium mixture of H_2 in AMS which contacts a short bed of 1.62×10^{-3} m dia. uniformly active 2.5% Pd/A_2O_3 catalyst pellets. The clear rate increase with decreasing flow rate, and hence wetting efficiency, demonstrates the enhancing influence of external mass transport of the H_2 on the nonwetted parts of the pellets.

A single-pellet partial wetting model was presented by the investigators that predicts an increasing effectiveness (or rate) with decreasing wetting efficiency. However, their model does not account for possible liquid reactant (AMS) depletion. As a result, the eventual rate decrease as $E_w \rightarrow 0$, conditions for which the nonvolatile liquid reactant is no longer supplied, cannot be predicted. Our analysis and modeling of the data addresses these two issues. However, we emphasize that the use of a single-pellet model to predict the performance of a differentially operated trickle-bed reactor is an approximation. This point is considered in the Discussion section.

The first step in computing the reaction rate as a function of liquid flow rate is to estimate the liquid flow rate range for which partial external wetting occurs. To do this we apply the dry patch model of Hartley and Murgatroyd (1964). The model assumes that this minimal mass flow rate per unit length, Γ, above which the surface is fully wetted is related to the fluid properties by

$$\Gamma = \xi \left(\frac{\mu\rho}{g}\right)^{1/5} \sigma^{3/5} \tag{55}$$

where ξ is a proportionality constant on the order of 0.1 (Norman and McIntyre, 1960), μ and ρ are the fluid viscosity and density, respectively, σ is the interfacial tension, and g is the acceleration due to gravity. The critical superficial liquid mass flow rate to attain complete wetting is determined for a packed bed by multiplying Γ by the total grain length boundary, ℓ, given by

$$\ell = \left[\frac{3\pi(1-\epsilon_r)}{2d_p}\right]\left(\frac{\pi d_r^2}{4}\right) \tag{56}$$

where ϵ_r is the bed void fraction, d_r is the reactor diameter, and d_p is the average pellet diameter (Ng, 1986). We assume that the wetting efficiency is given by the ratio of the actual flow rate q and $q^o = \Gamma\ell/\rho$; i.e.,

$$E_w = \frac{q}{q^o} \tag{57}$$

Thus, as the flow rate increases in the partial wetting regime, the liquid film spreads out over the available surface but maintains a constant depth. Moreover, we assume that the external mass transfer rates are independent of the flow rate in the partial wetting regime.

We computed q^o using estimates for the physical properties and other data provided by Herskowitz et al. These values are provided in Table 1. Assuming that the proportionality constant ξ is 0.1, we calculate $q^o = 6.31 \times 10^{-6}$ m^3/s. This demarcation between partial and complete wetting is denoted by a dashed line in Figure 13. This estimate is within the experimental flow rate range in which the global rate was observed to increase slightly with increasing q. This indicates that in this flow rate range the pellets are fully wetted and additional flow rate increases translate into an increased overall rate because of enhanced external mass transfer. Thus, our predicted q^o may be too high.

The second step is to compute the reaction rate r using Eq. 43. The solid line in Figure 13 is our model simulation of the data. Most of the input data were provided in the paper, including k, C_{Ae}, ρ, ϵ_p, and ρ_p. Values for D_{Ae} and D_{Be} were taken from literature experimental data. We convert the spherical geometry into the slab geometry by using $V_p/S_x = d_p/6$ as the uniformly active reaction zone thickness δ. The external component of the transport coefficients, k^o_{A1}, k^o_{A1}, k^o_{A2}, and k^o_B, Eqs. 17a–17e, were adjusted in order to fit the data approximately. We found $k^o_{A1} = 1.5 \times 10^{-4}$ m/s, $k^o_{A2} = 3.0 \times 10^{-4}$ m/s, and $k^o_B = 2.0 \times 10^{-4}$ m/s. These values are reasonable for several reasons:

1. The estimate for k^o_{A1}, the overall transport coefficient of hydrogen on the wetted part, 1.5×10^{-4} m/s, is close to values provided by others (Satterfield et al., 1968; Goto and Smith, 1975; Herskowitz et al. ,1979).

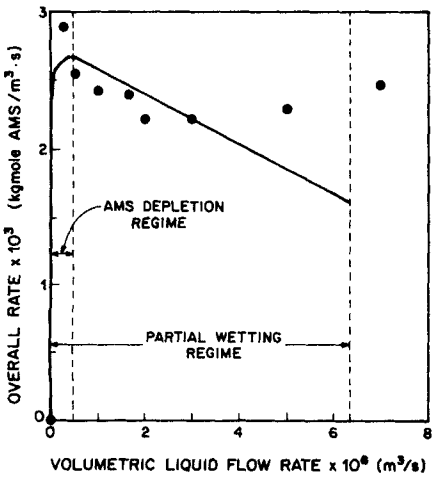

Figure 13. Model predictions of data of Herskowitz et al. (1979).
Parameter values given in Table 1.

Table 1. Parameter* Values Used in Qualitative Fit of Trickle-bed Reactor Data of Herskowitz et al. (1979), Figure 13

k	56.15 s^{-1}	σ	32.0×10^{-3} N/m
k^o_{A1}	1.5×10^{-4} m/s	g	9.8 m/s^2
k^o_{A2}	3.0×10^{-4} m/s	ρ	893 kg/m^3 liquid
k^o_B	2.0×10^{-4} m/s	d_p	1.62×10^{-3} m pellet
D_{Ae}	9.3×10^{-9} m^2/s	ϵ_p	0.5 m^3 void/m^3 pellet
D_{Be}	7.0×10^{-10} m^2/s	ϵ_r	0.48 m^3 void/m^3 reactor
C_{Bf}	7.5 kmol/m^3	d_r	2.54×10^{-2} m reactor
C_{Ae}	2.85×10^{-3} kmol/m^3	ρ_p	1,530 kg pellet/m^3 pellet
ν	1.0 kmol B/kmol A	ξ	0.1
μ	7.17×10^{-4} kg/m · s	δ	2.18×10^{-4} m

*Parameters defined in text or Notation

2. The estimate of 3.0×10^{-4} m/s for k^o_{A2}, the overall nonwetted part hydrogen mass transfer coefficient, is only slightly greater than k_{A1}. This follows directly from the experimental procedure of using an H_2-saturated AMS liquid feed. Hence, k^o_{A1} and k^o_{A2} should have similar magnitudes.

3. k^o_B, the overall wetted part AMS mass transfer coefficient, is larger than k^o_{A1} because the liquid feed contains a high AMS concentration. Thus, the external resistance to AMS transport is not as significant.

This data analysis demonstrates two points. First, these predictions convey the need to account for a depleting liquid reactant. Even though the ratio of AMS concentration in the liquid film to the equilibrium solubility of H_2 is extremely large (u_{Bf} = 2,631.6) the model predicts depletion of AMS within the pellet for wetting efficiencies (flow rates) below 0.074 (4.65×10^{-7} m^3/s). The reason for this is the active catalyst and slow AMS diffusion ($\phi = 156$). The predicted maximum rate is obtained close to the minimum liquid flow rate above which complete catalyst utilization is attained. As the flow rate is increased beyond this point the decreased supply rate of hydrogen on the wetted part causes a gradual rate decline. Second, the observed relative minimum in the rate cannot be predicted. We suspect that the mild rate increase for sufficiently large flow rates is a result of enhanced external mass transfer (as suggested by Herskowitz et al., 1979). Recall that our model includes no dependence of the mass transfer coefficients on the flow rate in the partial wetting regime. Moreover, the lack of agreement for E_w approaching unity may also be attributed both to experimental error and our approximate means of computing the flow rate range in which partial wetting occurs.

Discussion and Concluding Remarks

In addition to the demonstration of the interplay between partial wetting, the chemical reaction, and external and intraparticle transport resistances on effectiveness, the one-dimensional steady state model of a partially wetted catalytic pellet considers in detail two essential physical features that have not been emphasized previously. The first feature concerns a depleting liquid reactant. Physically, one expects that at steady state a low wetting efficiency will make it difficult to supply enough of the nonvolatile liquid reactant rapidly enough to all points within the pellet. The model predicts that B will deplete for a sufficiently active catalyst. Moreover, the physical requirement that the rate is zero as the wetting efficiency approaches zero is satisfied. A decreased transport rate of B, bulk liquid concentration of B, or diffusivity of B makes depletion more likely. Of course, the validity of a zero-order dependence on B for nonexcess B concentrations is questionable. For B concentrations below the stoichiometric requirement the dissolved gas reactant is no longer the limiting reactant and the rate dependence is likely to be of a nonzero order with respect to B. A more detailed model should incorporate this dependence. Even in this nonlinear case the liquid and dissolved gas reactants will be limiting, depending on the position within the pellet relative to the wetted zone (Funk et al., 1987).

The second essential feature is the prediction of an effectiveness maximum. A necessary condition for effectiveness enhancement by partial wetting is that transport of the gas reactant A must be more effective on the nonwetted than on the wetted part. It is interesting that the broadness of the effectiveness maximum depends on which rate process is controlling. Under conditions of reaction control the peak is broad as $\eta \simeq 1$, except as $E_w \to 0$ (e.g., $\phi = 1$ in Figure 5a). The peak is sharp under conditions in which external transport is controlling and a relatively low wetting efficiency is sufficient to supply B throughout the entire pellet. In this case there is a pronounced transition between two regimes (e.g., $\alpha Bi_{A2} = 10$ curve in Figure 4, $\phi = 10$ curve in Figure 5a). For $E_w < E^m_w$ the increasing dependence of η on E_w is a result of an increasing catalyst utilization s^*. Near the sharp maximum complete utilization ($s^* = 1$) is attained. Subsequent increases in E_w above E^m_w results in an effectiveness decrease because of the decreased supply rate of A through the liquid film. The effectiveness maximum is broad under conditions in which intraparticle diffusion limitations are severe and a relatively large E_w is required to supply B throughout the pellet (e.g., $\alpha Bi_{A2} > 100$ in Figure 4). In the region of η insensitivity, increases in E_w serve to increase the catalyst utilization, however this is offset by the very slow A and/or B intraparticle diffusion, which prevents an overall rate increase.

The model predicts that in all cases the wetting efficiency that gives the maximum effectiveness, E^m_w, is less than the minimal wetting efficiency necessary to supply B throughout the entire pellet, E^*_w. In many cases, however, $E^m_w \simeq E^*_w$. An exact determination of E^m_w requires the simultaneous solution of $F(s^*, E_w, p) = 0$ and

$$\frac{d\eta}{dE_w} = \left(\frac{\partial \eta}{\partial E_w}\right)_{s^*} + \left(\frac{\partial \eta}{\partial s^*}\right)_{E_w}\left(\frac{\partial s^*}{\partial E_w}\right) = 0 \tag{58}$$

where $(\partial\eta/\partial E_w)_{s^*}$ and $(\partial\eta/\partial s^*)_{E_w}$ are determined using Eqs. 45–46 and $\partial s^*/\partial E_w$ is found by implicit differentiation of $F(s^*, E_w, p) = 0$ (Appendices 3–4). Thus, the determination of $d\eta/dE_w$ is straightforward in principle but cumbersome algebra is expected in finding the three partial derivatives.

Although the model provides interesting insights into how the physical factors affect the effectiveness of a partially wetted catalyst, its applicability to modeling the performance of a trickle-bed reactor is limited by two key assumptions.

First, it is assumed that the intraparticle concentration of A and B in the direction normal to the flat surface is uniform. This is strictly valid for reactions that occur within a thin layer of impregnated support coated on an impermeable support (washcoated catalyst) and that satisfy the criterion of Eq. 2. We have shown that our model can be extended to approximate cases in which intraparticle concentration gradients exist within the washcoat in the direction normal to the wetted surface. In addition, the one-dimensional model approximates the behavior of surface shell impregnated porous catalysts. It is expected that under some conditions the reactants may exchange between the nonwetted and wetted regions by diffusion through the inert, permeable core. The model does not account for this diffusion process. This communication would provide an enhanced supply rate of A into the wetted region. This contribution may be lumped into k_{A1}. Diffusion of B through the inert core may make its depletion less likely when the overall rate is not limited by the supply rate of B. However, the increased supply rate of A to the wetted region counteracts this. Only the numerical solution of the two-dimensional model with the same kinetics can check the importance of this exchange process for the surface shell catalyst. Finally, we have shown that the model also approximates the behavior of uniformly active catalysts. The model predicts the correct overall rate in the case of complete wetting with

severe intraparticle diffusion limitations. Moreover, the excellent agreement with exact two-dimensional model predictions under conditions of no B depletion demonstrates the utility and generality of the one-dimensional model. Considering these facts, its novel accounting for liquid reactant depletion, and its computational efficiency over its two-dimensional model counterparts, the one-dimensional model is a good candidate for incorporation into heterogeneous trickle-bed reactor models.

Second, it is assumed that the wetting of the catalytic pellet is in the form of a flowing liquid film; however, other flow features—rivulets, pendular structures, liquid pockets—are also present. A detailed trickle-bed reactor analysis should incorporate the single-pellet model into a reactor model that predicts the spatial heterogeneity of the wetting efficiency as a function of the operating conditions. Moreover, uncertainty about the transition to partial wetting and of the external mass transfer features of partially wetted catalysts signals a need for fundamental single-pellet experiments. Efforts to relax the model assumptions are currently under way and extension of the model to investigate selectivity enhancement and nonisothermal effects are also in progress.

Acknowledgment

The authors are grateful for the partial support of this research by NSF grant No. CBT-8700554.

Notation

A = gaseous reactant
B = liquid reactant
Bi^o = Biot number based on external transport coefficients, Eq. 17e
Bi = Biot number based on overall transport coefficient Eq. 7
C = liquid phase concentration
C_{Ay}, C_{By} = intraparticle A and B concentrations ignoring x direction
$\hat{C}_{Ay}, \hat{C}_{By}$ = average (with respect to y direction) A and B intraparticle concentrations
d = diameter
D_{Ae}, D_{Be} = effective diffusivities for A, B
E_w = wetting efficiency
g = acceleration due to gravity
k = rate constant
k_A, k_B = overall mass transfer coefficients for A, B
k_A^o, k_B^o = external components of overall mass transfer coefficients
K_j = jth integration constant
ℓ = grain length boundary
L = pellet length
m = parameter, Eq. 7
p = vector of model parameters
p_{bA} = bulk partial pressure of A
q = liquid volumetric flow rate
r = reaction rate
s = dimensionless distance in direction parallel to pellet surface
S = pellet width
S_x = external surface area of catalyst
s^* = dimensionless distance at which B depletes (catalyst utilization)
u = dimensionless concentration
V_p = volume of catalyst
x = direction parallel to pellet surface
y = direction normal to pellet surface
z = flow direction of liquid film

Greek letters

α = aspect ratio of catalyst, Eq. 7
β = parameters, Appendix 1
γ_1, γ_2 = parameters, Appendix 1
Γ = minimal mass flow rate per unit length for complete wetting
δ = thickness of active zone
δ_A^*, δ_B^* = diffusion lengths, Eq. 12
ϵ = void fraction or quantity, Eq. 12b
η = catalyst effectiveness
μ = liquid viscosity
ν = stoichiometric coefficient
ξ = proportionality constant, Eq. 55
ρ = liquid density or parameters, Appendix 1
σ = interfacial tension
ϕ = Thiele modulus based on catalyst half-width
ϕ_y = Thiele modulus based on thickness of active layer

Subscripts

act = active
A = gaseous reactant
b = bulk
B = liquid reactant
e = effective or equilibrium
f = film
gl = gas-to-liquid
gs = gas-to-solid
i = interfacial
ls = liquid-to-solid
p = pellet
r = reactor
s = surface
w = wetting
y = y direction
1, 2, 3 = region 1, 2, 3

Superscripts

$*$ = point of B depletion for s^* or diffusion length δ^*
m = maximum
o = critical or external transport component of overall transport coefficients

Appendix 1: General Solutions to the Four Cases

Case I, $s^* > 1$

$$u_{A1}(s) = K_1 \sinh(\rho_{A1}s) + K_2 \cosh(\rho_{A1}s) + \frac{\beta_{A1}^2}{\rho_{A1}^2} \tag{1.A}$$

$$u_{B1}(s) = K_3 \sinh(\rho_B s) + K_4 \cosh(\rho_B s) + \frac{m\phi^2 K_1}{\rho_{A1}^2 - \rho_B^2}[\cosh(\rho_B s) - \cosh(\rho_{A1}s)] + \frac{m\phi^2 K_2}{\rho_{A1}^2 - \rho_B^2}[\cosh(\rho_{A1}s) - \cosh(\rho_B s)] + \frac{\gamma_1}{\rho_B^2}[\cosh(\rho_B s) - 1] \tag{1.B}$$

$$u_{A2}(s) = K_5 \cosh(\rho_{A2}s) + K_6 \cosh[\rho_{A2}(1 - s)] + \frac{\beta_{A2}^2}{\rho_{A2}^2} \tag{1.C}$$

$$u_{B2}(s) = \frac{m\phi^2}{\rho_{A2}^2}\left\{K_5 \cosh(\rho_{A2}s) + K_6 \cosh[\rho_{A2}(1 - s)] + \frac{\beta_{A2}^2 s^2}{2}\right\} + K_7 s + K_8 \tag{1.D}$$

Case II, $E_w < s^* < 1$

$u_{A1}(s)$: Eq. 1.A

$u_{B1}(s)$: Eq. 1.B

$u_{A2}(s)$: Eq. 1.C

$u_{B2}(s)$: Eq. 1.D

$$u_{A3}(s) = K_9 \cosh(\beta_{A3}s) + K_{10}\cosh[\beta_{A3}(1-s)] + 1 \quad (1.E)$$

$$u_{B3}(s) = 0 \quad (1.F)$$

Case III, $0 < s^* < E_w$

$u_{A1}(s)$: Eq. 1.A

$u_{B1}(s)$: Eq. 1.B

$$u_{A2}(s) = K_5 \cosh(\beta_{A1}s) + K_6 \cosh[\beta_{A1}(1-s)] - \frac{\gamma_2}{\beta_{A1}^2} \quad (1.G)$$

$$u_{B2}(s) = 0 \quad (1.H)$$

$$u_{A3}(s) = K_9 \cosh(\beta_{A3}s) + K_{10}\cosh[\beta_{A3}(1-s)] + 1 \quad (1.I)$$

$$u_{B3}(s) = 0 \quad (1.J)$$

Case IV, $s^* < 0$

$u_{A1}(s)$: Eq. 1.G

$u_{A2}(s)$: Eq. 1.I

Definitions of terms:

$$\beta_{A1}^2 = \alpha Bi_{A1} \qquad \beta_{A2}^2 = \alpha Bi_{A2}$$

$$\beta_{A3}^2 = \alpha Bi_{A3} \qquad \rho_B^2 = \alpha Bi_B$$

$$\rho_{A1}^2 = \phi^2 + \beta_{A1}^2 \qquad \rho_{A2}^2 = \phi^2 + \beta_{A2}^2$$

$$\gamma_1 = \frac{m\phi^2\beta_{A1}^2}{\rho_{A1}^2} - \beta_B^2 u_{Bf} \qquad \gamma_2 = \frac{\rho_B^2 u_{Bf}}{m} - \beta_{A1}^2$$

Appendix 2: Expressions for Eight Integration Constants for Case of Nondepleting *B*

Species A

$$K_1 = K_5 = 0$$

$$K_6 = \frac{\phi^2(\beta_{A1}^2 - \beta_{A2}^2)}{\rho_{A1}^2\rho_{A2}^2\cosh[\rho_{A2}(1-E_w)]\left\{1 + \dfrac{\rho_{A2}\tanh[\rho_{A2}(1-E_w)]}{\rho_{A1}\tanh(\rho_{A1}E_w)}\right\}}$$

$$K_2 = -\left\{\frac{\rho_{A2}\sinh[\rho_{A2}(1-E_w)]}{\rho_{A1}\sinh(\rho_{A1}E_w)}\right\}K_6$$

Species B

$$K_3 = 0 \qquad K_7 = -\frac{m\phi^2\beta_{A2}^2}{\rho_{A2}^2}$$

$$K_1 = \left(\frac{m\phi^2}{\rho_{A2}^2 - \rho_B^2}\right)\left[1 - \frac{\rho_{A1}\sinh(\rho_{A1}E_w)}{\rho_B\sinh(\rho_BE_w)}\right]K_2 - \frac{\gamma_1}{\rho_B^2} - \frac{m\phi^2}{\sinh(\rho_BE_w)}\left(\left\{\frac{\sinh[\rho_{A2}(1-E_w)]}{\rho_{A2}\rho_B}\right\}K_6 + \frac{(1-E_w)\beta_{A2}^2}{\rho_{A2}^2\rho_B}\right)$$

$$K_8 = \left[\frac{m\phi^2\cosh(\rho_{A1}E_w)}{\rho_{A1}^2 - \rho_B^2}\right]\left[1 - \frac{\rho_{A1}\tanh(\rho_{A1}E_w)}{\rho_B\tanh(\rho_BE_w)}\right]K_2 - \frac{\gamma_1}{\rho_B^2} - m\phi^2\cosh[\rho_{A2}(1-E_w)]\left\{\frac{1}{\rho_{A2}^2} + \frac{\tanh[\rho_{A2}(1-E_w)]}{\rho_{A2}\rho_B\tanh(\rho_BE_w)}\right\}K_6 + \frac{m\phi^2\beta_{A2}^2}{\rho_{A2}^2}\left[E_w\left(1 - \frac{E_w}{2}\right) - \frac{(1-E_w)}{\rho_B\tanh(\rho_BE_w)}\right]$$

Appendix 3: Expressions for Ten Integration Constants and Implicit Function of s^* for Case of Depleting *B* in Nonwetted Zone

$$K_1 = K_3 = K_9 = 0 \qquad K_{10} = \frac{D_3D_4 - D_2D_5}{D_6 + D_7}$$

where

$$D_3 = D_2 - \frac{\phi^2}{\rho_{A2}^2\cosh(\rho_{A2}s^*)}$$

$$D_2 = \frac{\phi^2(\beta_{A1}^2 - \beta_{A2}^2)}{\rho_{A1}^2\rho_{A2}^2\cosh(\rho_{A2}E_w)\left[1 - \dfrac{\rho_{A2}\tanh(\rho_{A2}E_w)}{\rho_{A1}\tanh(\rho_{A1}E_w)}\right]}$$

$$D_4 = D_1 - \frac{\sinh[\rho_{A2}(1-s^*)]}{\sinh(\rho_{A2}s^*)}$$

$$D_1 = -\frac{\left\{\dfrac{\cosh[\rho_{A2}(1-E_w)]}{\cosh(\rho_{A2}E_w)} + \dfrac{\rho_{A2}\sinh[\rho_{A2}(1-E_w)]}{\rho_{A1}\cosh(\rho_{A2}E_w)\tanh(\rho_{A1}E_w)}\right\}}{\left[1 - \dfrac{\rho_{A2}\tanh(\rho_{A2}E_w)}{\rho_{A1}\tanh(\rho_{A1}E_w)}\right]}$$

$$D_5 = D_1 + \frac{\cosh[\rho_{A2}(1-s^*)]}{\cosh(\rho_{A2}s^*)} \qquad D_6 = \frac{\cosh[\beta_{A3}(1-s^*)]}{\cosh(\rho_{A2}s^*)}D_4$$

$$D_7 = \frac{\beta_{A3}\sinh[\beta_{A3}(1-s^*)]}{\rho_{A2}\sinh(\rho_{A2}s^*)}D_5$$

$$K_6 = \frac{\dfrac{\cosh[\beta_{A3}(1-s^*)]}{\cosh(\rho_{A2}s^*)}K_{10} - D_3}{D_5} \qquad K_5 = D_1K_6 + D_2$$

$$K_2 = \frac{\cosh(\rho_{A2}E_w)}{\cosh(\rho_{A1}E_w)}K_5 + \frac{\cosh[\rho_{A2}(1-E_w)]}{\cosh(\rho_{A1}E_w)}K_6 + \frac{\phi^2(\beta_{A2}^2 - \beta_{A1}^2)}{\rho_{A1}^2\rho_{A2}^2\cosh(\rho_{A1}E_w)}$$

$$K_7 = \frac{m\phi^2}{\rho_{A2}}\left\{\sinh[\rho_{A2}(1-s^*)]K_6 - \sinh(\rho_{A2}s^*)K_5 - \frac{\beta_{A2}^2s^*}{\rho_{A2}}\right\}$$

$$K_8 = -\left(\frac{m\phi^2}{\rho_{A2}^2}\right)\left\{[\cosh(\rho_{A2}s^*)]K_5 + \cosh[\rho_{A2}(1-s^*)]K_6 + \frac{\beta_{A2}^2(s^*)^2}{2}\right\} - s^*K_7$$

$$K_4 = \frac{m\phi^2}{\rho_{A2}^2}\left(\left[\frac{\cosh(\rho_{A2}E_w)}{\cosh(\rho_BE_w)}\right]K_5 + \left\{\frac{\cosh[\rho_{A2}(1-E_w)]}{\cosh(\rho_BE_w)}\right\}K_6 + \frac{\beta_{A2}^2E_w^2}{2\cosh(\rho_BE_w)}\right) + \left(\frac{m\phi_2}{\rho_{A1}^2 - \rho_B^2}\right)\left[1 - \frac{\cosh(\rho_{A1}E_w)}{\cosh(\rho_BE_w)}\right]K_2 + \left[\frac{E_w}{\cosh(\rho_BE_w)}\right]K_7 + \left[\frac{1}{\cosh(\rho_BE_w)}\right]K_8 - \frac{\gamma_1}{\rho_B^2}\left[1 - \frac{1}{\cosh(\rho_BE_w)}\right]$$

$$F(s^*, E_w, p) = K_4 + \left(\frac{m\phi^2}{\rho_{A1}^2 - \rho_B^2}\right)\left[\frac{\rho_{A1}\sinh(\rho_{A1}E_w)}{\rho_B \sinh(\rho_B E_w)} - 1\right]K_2 + \frac{\gamma_1}{\rho_B^2} - \left[\frac{1}{\rho_B \sinh(\rho_B E_w)}\right]K_7 - \frac{m\phi^2}{\rho_{A2}\rho_B}\left\{\frac{\sinh(\rho_{A2}E_w)}{\sinh(\rho_B E_w)}K_5 - \frac{\sinh[\rho_{A2}(1-E_w)]}{\sinh(\rho_B E_w)}K_6 + \frac{\beta_{A2}^2 E_w}{\rho_{A2}\sinh(\rho_B E_w)}\right\} = 0$$

Appendix 4: Expressions for Eight Integration Constants and Implicit Function of s^* for Case of Depletion of B in Wetted Zone

$$K_1 = K_3 = K_9 = 0$$

$$K_6 = \frac{D_7 D_3 - D_1 D_5}{D_2 D_7 + D_1 D_4 + D_1 D_6}$$

$$K_5 = \frac{D_3}{D_1} - \frac{D_2}{D_1}K_6$$

$$K_2 = D_4 K_6 + D_5$$

$$K_4 = \frac{\gamma_1}{\rho_B^2}\left[\frac{1}{\cosh(\rho_B s^*)} - 1\right] + \left(\frac{m\phi^2}{\rho_{A1}^2 - \rho_B^2}\right)\left[1 - \frac{\cosh(\rho_{A1}s^*)}{\cosh(\rho_B s^*)}\right]K_2$$

$$K_{10} = \frac{\beta_{A1}\sinh[\beta_{A1}(1-E_w)]}{\beta_{A2}\sinh[\beta_{A2}(1-E_w)]}K_6 - \frac{\beta_{A1}\sinh[\beta_{A1}E_w)}{\beta_{A2}\sinh[\beta_{A2}(1-E_w)]}K_5$$

where

$$D_1 = \frac{\cosh(\beta_{A1}E_w)}{\cosh[\beta_{A2}(1-E_w)]} + \frac{\beta_{A1}\sinh(\beta_{A1}E_w)}{\beta_{A2}\sinh[\beta_{A2}(1-E_w)]}$$

$$D_2 = \frac{\cosh[\beta_{A1}(1-E_w)]}{\cosh[\beta_{A2}(1-E_w)]} - \frac{\beta_{A1}\sinh[\beta_{A1}(1-E_w)]}{\beta_{A2}\sinh[\beta_{A2}(1-E_w)]}$$

$$D_3 = \left(\frac{\gamma_2}{\beta_{A1}^2} + 1\right)\frac{1}{\cosh[\beta_{A2}(1-E_w)]}$$

$$D_4 = \frac{\cosh[\beta_{A1}(1-s^*)]}{\cosh(\rho_{A1}s^*)} - \frac{\cosh(\beta_{A1}s^*)}{\cosh(\rho_{A1}s^*)}\frac{D_2}{D_1}$$

$$D_5 = \frac{\cosh(\beta_{A1}s^*)D_3}{\cosh(\rho_{A1}s^*)D_1} - \left(\frac{\gamma_2}{\beta_{A1}^2} + \frac{\beta_{A1}^2}{\rho_{A1}^2}\right)\frac{1}{\cosh(\rho_{A1}s^*)}$$

$$D_6 = \frac{\beta_{A1}\sinh[\beta_{A1}(1-s^*)]}{\rho_{A1}\sinh(\beta_{A1}s^*)} \qquad D_7 = \frac{\beta_{A1}\sinh(\beta_{A1}s^*)}{\rho_{A1}\sinh(\rho_{A1}s^*)}$$

$$F(s^*, E_w, p) = \left(\frac{m\phi^2}{\rho_{A1}^2 - \rho_B^2}\right)\left(\frac{\rho_{A1}\sinh(\rho_{A1}s^*)}{\rho_B} - 1\right) + \frac{\gamma}{\rho_B^2} + K_4 = 0$$

Appendix 5: Expressions for Integrals Appearing in Effectiveness Formula

B depletion in nonwetted part

$$\int_0^{E_w} u_{A1}\,ds = \frac{K_1}{\rho_{A1}}[\cosh(\rho_{A1}E_w) - 1] + \frac{K_2}{\rho_{A2}}\sinh(\rho_{A1}E_w) + \frac{E_w\beta_{A1}^2}{\rho_{A1}^2} \quad (5.A)$$

$$\int_{E_w}^{s^*} u_{A2}\,ds = \frac{K_5}{\rho_{A2}}[\sinh(\rho_{A2}s^*) - \sinh(\rho_{A2}E_w)] - \frac{K_6}{\rho_{A2}}\{\sinh[\rho_{A2}(1-s^*)] - \sinh[\rho_{A2}(1-E_w)]\} + \frac{\beta_{A2}^2}{\rho_{A2}^2}(s^* - E_w) \quad (5.B)$$

$$\int_{s^*}^1 u_{A3}\,ds = \frac{K_9}{\beta_{A3}}[\sinh(\beta_{A3}) - \sinh(\beta_{A3}s^*)] + \frac{K_{10}}{\beta_{A3}}\sinh[\beta_{A3}(1-s^*)] + 1 - s^* \quad (5.C)$$

The constants are given by expressions in Appendix 3.

B depletion in wetted part

$$\int_0^{s^*} u_{A1}\,ds = \frac{K_1}{\rho_{A1}}[\cosh(\rho_{A1}s^*) - 1] + \frac{K_2}{\rho_{A2}}\sinh(\rho_{A1}s^*) + \frac{s^*\beta_{A1}^2}{\rho_{A1}^2} \quad (5.D)$$

$$\int_{s^*}^{E_w} u_{A2}\,ds = \frac{K_5}{\beta_{A1}}[\sinh(\beta_{A1}E_w) - \sinh(\beta_{A1}s^*)] - \frac{\gamma_2}{\beta_{A1}^2}(E_w - s^*) \quad (5.E)$$

$$+ \frac{K_6}{\beta_{A1}}\{\sinh[\beta_{A1}(1-s^*)] - \sinh[\beta_{A1}(1-E_w)]\}$$

$$\int_{E_w}^1 u_{A3}\,ds = \frac{K_9}{\beta_{A2}}[\sinh(\beta_{A3}) - \sinh(\beta_{A3}E_w)] + K_{10}\sinh[\beta_{A3}(1-E_w)] + 1 - E_w \quad (5.F)$$

The constants are given by expressions in Appendix 4.

Literature Cited

Babcock, B. D., G. T. Mejdell, and O. A. Hougen, "Catalyzed Gas-Liquid Reactions in Trickle-Bed Reactors," *AIChE J.*, **3**, 366 (1957).

Beaudry, E., M. P. Dudukovic, and P. L. Mills, "Trickle-Bed Reactors: Liquid Diffusional Effects in a Gas-Limited Reaction," *AIChE J.*, **33**(9), p. 1435 (Sept., 1987).

El-Hisnawi, A. A., M. P. Dudukovic, and P. L. Mills, "Trickle-Bed Reactors: Dynamic Tracer Tests, Reaction Studies, and Modeling of Reactor Performance," *Am. Chem. Soc. Symp. Ser.*, **196**, 421 (1982).

Froment, G. F. and K. B. Bischoff, *Chemical Reactor Analysis and Design*, Wiley, New York (1979).

Funk, G. A., M. P. Harold, and K. M. Ng, to *AIChE J.* (1987).

Gates, B. C., J. R. Katzer, and G. C. A. Schuit, *Chemistry of Catalytic Processes*, McGraw-Hill, New York (1979).

Germain, A., M. Crine, P. Marchot, and G. A. L'Homme, "Modeling of a Trickle-Bed Reactor: The Hydrogenation of 2-Butanone on a Ruthenium Catalyst," *Am. Chem. Soc. Symp. Ser.*, **65**, 411 (1978).

Goto, S., A. Lakota, and J. Levec, "Effectiveness Factors of *n*th-Order Kinetics in Trickle-Bed Reactors," *Chem. Eng. Sci.*, **36**, 157 (1981).

Goto, S. and J. M. Smith, "Trickle-Bed Reactor Performance. I: Holdup and Mass Transfer Effects," *AIChE J.*, **21**, 706 (1975).

Hartley, D. E., and W. Murgatroyd, "Criteria for the Break-up of Thin Liquid Layers Flowing Isothermally Over a Solid Surface," *Int. J. Heat Mass Transfer*, **7**, 1003 (1964).

Herskowitz, M., "Wetting Efficiency in Trickle-Bed Reactors. The

Overall Effectiveness Factor of Partially Wetted Catalyst Particles," *Chem. Eng. Sci.*, **36**, 1665 (1981).
Herskowitz, M., R. G. Carbonell, and J. M. Smith, "Effectiveness Factor and Mass Transfer in Trickle-Bed Reactors," *AIChE J.*, **25**, 272 (1979).
Mata, A. R., and J. M. Smith, "Oxidation of Sulfur Dioxide in a Trickle-Bed Reactor," *Chem. Eng. J.*, **22**, 229 (1981).
Mills, P. L., and M. P. Dudukovic, "A Dual-Series Solution for the Effectiveness Factor of Partially Wetted Catalysts in Trickle-Bed Reactors," *Ind. Eng. Chem. Fundam.*, **18**, 139 (1979).
Morita, S., and J. M. Smith, "Mass Transfer and Contacting Efficiency in a Trickle-Bed Reactor," *Ind. Eng. Chem. Fundam.*, **17**, 113 (1978).
Ng, K. M., "A Model for Flow Regime Transitions in Cocurrent Downflow Trickle-Bed Reactors," *AIChE J.*, **32**, 115 (1986).
Norman, W. S., and V. McIntyre, "Heat Transfer to a Film on a Vertical Surface," *Trans. Inst. Chem. Eng.*, **38**, 301 (1960).
Ramachandran, P. A., and J. M. Smith, "Effectiveness Factors in Trickle-Bed Reactors," *AIChE J.*, **25**, 538 (1979).
Ring, Z. E., and R. W. Missen, "Trickle-Bed Reactors: Effect of Wetting Geometry on Overall Effectiveness Factor," *Can. J. Chem. Eng.*, **64**, 117 (1986).
Sakornwimon, W. and N. D. Sylvester, "Effectiveness Factors for Partially Wetted Catalysts in Trickle-Bed Reactors," *Ind. Eng. Chem. Process Des. Dev.*, **21**, 16 (1982).
Sato, Y., T. Hirose, F. Takahashi, M. Toda, and Y. Hashiguchi, "Flow Pattern and Pulsation Properties of Cocurrent Gas-Liquid Downflow in Packed Beds," *J. Chem. Eng. Japan.* **6**, 315 (1973).
Satterfield, C. N., A. A. Pelossof, and T. K. Sherwood, "Mass Transfer Limitations in a Trickle-Bed Reactor," *AIChE J.*, **15**, 226 (1968).
Schwartz, J. G., E. Weger, and M. P. Dudukovic, "A New Tracer Method for Determination of Liquid-Solid Contacting Efficiency in Trickle-Bed Reactors," *AIChE J.*, **22**, 894 (1976).
Sedricks, W., and C. N. Kenney, "Partial Wetting in Trickle-Bed Reactors: The Reduction of Crotonaldehyde Over a Palladium Catalyst," *Chem. Eng. Sci.*, **28**, 559 (1973).
Tan, C. S., and J. M Smith, "Catalyst Particle Effectiveness with Unsymmetrical Boundary Conditions," *Chem. Eng. Sci.*, **35**, 1601 (1980).
Turek, F., and R. Lange, "Mass Transfer in Trickle-Bed Reactors at Low Reynolds Number," *Chem. Eng. Sci.*, **36**, 569 (1981).
Zimmerman, S. P., and K. M. Ng, "Liquid Distribution in Trickling Flow Trickle-Bed Reactors," *Chem. Eng. Sci.*, **41**, 861 (1986).

Manuscript received Oct. 24, 1986, and revision received Apr. 8, 1987.

See NAPS document no. 04521 for 4 pages of supplementary material. Order from NAPS c/o Microfiche Publications, P.O. Box 3513, Grand Central Station, New York, NY 10163. Remit in advance in U.S. funds only $7.75 for photocopies or $4.00 for microfiche. Outside the U.S. and Canada, add postage of $4.50 for the first 20 pages and $1.00 for each of 10 pages of material thereafter, $1.50 for microfiche postage.